Geophysical Journal International

Geophys. J. Int. (2025) **243,** 1–25
Advance Access publication 2025 July 24
Geodynamics and Tectonics

https://doi.org/10.1093/gji/ggaf281

A new subsurface temperature model for Ireland from joint geophysical–petrological inversion of seismic, surface heat flow and petrophysical data

Emma L. Chambers [1], Javier Fullea [1,2], Duygu Kiyan [1,3], Sergei Lebedev [1,4], Christopher J. Bean [1,3], Patrick A. Meere [3,5], J. Stephen Daly [6,3,7], Nicola Willmot Noller [6], Robert Raine [8], Sarah Blake [9] and Brian M. O'Reilly [1,3]

[1] *School of Cosmic Physics, Dublin Institute for Advanced Studies, D02 Y006, Dublin, Ireland E-mail: echambers@cp.dias.ie*
[2] *Department of Physics of the Earth and Astrophysics, Universidad Complutense de Madrid, 28040, Madrid, Spain*
[3] *iCRAG, Research Ireland Centre for Applied Geosciences, D04 V1W8, Dublin, Ireland*
[4] *Department of Earth Sciences, University of Cambridge, CB3 0EZ, Cambridge, UK*
[5] *School of Biological, Earth and Environmental Sciences, University College Cork, T23 N73K, Cork, Ireland*
[6] *UCD School of Earth Sciences, University College Dublin, D04 V1W8, Dublin, Ireland*
[7] *UCD Earth Institute, University College Dublin, D04 V1W8, Dublin, Ireland*
[8] *Geological Survey of Northern Ireland, British Geological Survey, BT2 8FD, Belfast, UK*
[9] *Geological Survey Ireland, A94 N2R6, Dublin, Ireland*

Accepted 2025 July 17. Received 2025 June 26; in original form 2024 October 29

SUMMARY

High-quality maps of subsurface temperature and the geothermal gradient are useful when assessing the geothermal potential of a region. However, determining geothermal potential is a challenge when direct measurements of *in-situ* temperature and thermal property information are sparse and indirect geophysical methods are sensitive to a range of parameters, not just temperature. Here, we produce subsurface temperature maps of Ireland using a joint geophysical–petrological inversion, where seismic and other geophysical and petrophysical data are inverted directly for temperature in 1-D columns and are collated into a pseudo 3-D temperature volume. Additionally, the inversion produces new models for Moho and LAB depth and for the average crustal radiogenic heat production.

To assess the robustness of the resulting temperature model, an uncertainty analysis has been performed by inverting all of the 1-D columns for a range of reasonable input parameters applicable to the Irish crust (rather than the 'best' input parameters). The resulting uncertainty model suggests temperature estimates at 2 km depth in our model could vary by $\pm$ 2 to 5 °C with an average of 3.5 °C in most locations. The uncertainty model can be used to assess confidence in different regions of the temperature model. In addition, 3-D forward modelling was performed to assess the lateral heat flow variations when compared to the purely 1-D inversion. The upper-crustal geothermal gradient ranges from 20 to 40 °C km^{-1} indicating a higher geothermal gradient for Ireland than previously reported with subsurface temperatures at 2 km depth $>$ 60 °C everywhere, sufficient for residential and industrial heating purposes. The temperature gradient is typically higher in areas with thinner lithosphere. However, in some locations, the observed geotherms are elevated further due to high radiogenic heat production in granitic rocks. In Northern Ireland, a thin lithosphere, coupled with a weakly conductive basalt layer overlying warm crust, results in elevated temperatures. These are the first temperature maps for Ireland that include uncertainty estimates, providing ranges for the subsurface temperature values, and demonstrate that the maps are comparable to direct independent borehole temperature measurements, which are observed to fall within the model uncertainty. Our new methodology provides workflows for determining the geothermal potential in areas with limited direct temperature measurements. The final temperature model with uncertainty provides useful constraints for geothermal exploration and utilization on the island of Ireland.

Key words: Joint inversion; Heat flow; Crustal structure; Heat generation and transport.

1 INTRODUCTION

An important parameter when assessing a geothermal resource is the subsurface temperature and geothermal gradient which, traditionally, has been derived directly from borehole measurements. Knowing the depth to reach a certain temperature is a key issue in geothermal prospecting where greater drilling depth is often the costliest element of developing a geothermal site. However, in areas with few deep boreholes (defined as >1000 m deep), there is uncertainty and limited knowledge of the subsurface properties. The island of Ireland (This includes both Northern Ireland and the Republic of Ireland) is one such example having ∼42 deep boreholes with only 25 of these having temperature measurements (Northern Ireland: 17 total deep wells, 11 with temperature information, Republic of Ireland: 25 deep wells with temperature measurements at 14) (Goodman *et al.* 2004; Geological Survey Ireland 2020; Fellgett & Monaghan 2024). When assessing an area's geothermal potential and developing projects for future exploration and development, a 3-D temperature model is beneficial, rather than disparate point measurements, because rapid variations in subsurface geology can make lateral interpolation highly uncertain. This 3-D knowledge is useful in order to develop renewable resources to meet the Republic of Ireland's and Northern Ireland's climate action plans, to comply with the EU 2030 framework of climate and energy, and to meet global climate targets (European Council 2014; DECC 2020, 2024; DfE 2021).

To overcome limitations in available direct temperature measurements, it is possible to use indirect geophysical methods to model subsurface temperature. A coherent characterization of the geothermal gradient near the surface implies a bottom to top heat flow approach where knowledge of the thermal thickness of the lithosphere (or lithosphere–asthenosphere boundary, LAB), the crust–mantle boundary (Moho) and crustal lithology [thermal conductivity (TC) and radiogenic heat production (RHP)] are essential (Cammarano *et al.* 2003; Afonso *et al.* 2008; Scheck-Wenderoth & Maystrenko 2013; Fullea *et al.* 2021; Kassa *et al.* 2022; Chambers *et al.* 2023; Lebedev *et al.* 2024).

Seismic data can provide information on the geological boundaries within the Earth and recent deployments in Ireland have produced new surface wave velocity models which are sensitive to these boundaries (Bonadio *et al.* 2021; Chambers *et al.* 2023). Recent thermal property data sets have also been collated to produce laterally continuous models for TC in sediments and the upper crust (Chambers *et al.* 2023), and for RHP (Willmot Noller & Daly 2015). To produce a subsurface temperature map for all of Ireland, input data sets are required to cover each point in the model across the island of Ireland. This includes point measurements which have been interpolated in previous studies [e.g. surface heat flow (SHF), Mather *et al.* (2018)].

In this study we use the workflow of the joint geophysical–petrological inversion described in Chambers *et al.* (2023). The previous work used six points across the island of Ireland which had reliable input data for SHF, TC, RHP and elevation, which were used to parametrize a joint geophysical–petrological inversion for temperature. Six additional points at the locations of deep boreholes with temperature information were then inverted in the same way. The modelled temperature was compared to the measured temperature profiles, finding similar results between the model and observed data.

Here, we advance the previous study by producing a temperature model by inverting 1-D columns across the island of Ireland at a 0.2° x 0.2° lateral resolution and 1 km in depth. The 1-D columns were collated to produce a pseudo 3-D temperature model with uncertainty (pseudo in the sense that 1-D columns have been separately inverted and collated rather than a full 3-D inversion) from the surface to the base of the lithosphere, in addition to new maps of the Moho, LAB and crustal RHP. The input data sets have been taken as a series of interpolated grids rather than relying on point measurements at locations with a borehole, as was done in the previous study of Chambers *et al.* (2023). A significant addition is the uncertainty analysis [not carried out in Chambers *et al.* (2023)] to assess the possible variations in the final model, which was performed by running multiple 1-D inversions at every point to cover the ranges for the input parameters, rather than fixed values. The final pseudo 3-D uncertainty model then indicates the likely variation at every point across the island of Ireland, allowing future users to assess the confidence of a value when using this resource.

The new temperature maps suggest that subsurface temperatures at 2 km depth, are >45 °C everywhere across the island of Ireland with most areas above 60 °C. The warmest temperatures are present in areas with large granitic bodies exposed at the surface with high radiogenic signatures, and in Northern Ireland beneath the basalts of the Antrim Lava Group, which is likely to act as an insulating blanket, and is coupled with the thinnest lithosphere on the island of Ireland. The uncertainty analysis shows the variation in each point of the temperature maps providing ranges for the possible temperature values. The new temperature maps could be useful for future geothermal energy development in Ireland. This paper provides a proof of concept of the workflow and methodology that can be applied to other locations with sparse direct temperature measurements and limited subsurface data sets.

1.1 Deep geothermal studies in Europe

Previous studies have mapped lithospheric-scale thermal properties and the geothermal gradient using a variety of geophysical and geological data sets, and a range of modelling techniques across a variety of environments and scales (e.g. Cloetingh *et al.* 2010; Scheck-Wenderoth *et al.* 2014; Poulsen *et al.* 2015; Freymark *et al.* 2017; Lenkey *et al.* 2017; Békési *et al.* 2018; Anikiev *et al.* 2019; Majorowicz *et al.* 2019; Frey *et al.* 2022; Torne *et al.* 2023). The number of geothermal projects exploiting geothermal resources from depths >400 m is rising. Within Europe multiple projects are investigating the deep geothermal potential in areas such as Denmark (Poulsen *et al.* 2015, 2017), the Netherlands (Békési *et al.* 2020), the Upper Rhine Graben (Ledésert & Hébert 2020; Frey *et al.* 2022), throughout the entirety of Turkey for both heat and electricity (Mertoglu *et al.* 2019; Serpen & DiPippo 2022) and the Alpine–Pannonian transition zone (Lenkey *et al.* 2017). These are all well-established geothermal areas, but not high-enthalpy geothermal settings when compared to volcanic regions such as Iceland and Italy. In Iceland, improvements in technology now allow geothermal energy to be extracted from a variety of locations including those with lower temperatures, from greater depths to access higher temperatures and from non-conventional reservoirs such as supercritical geothermal (Fridleifsson & Elders 2005; Axelsson *et al.* 2010). Due to heat sources coming from both the crust and mantle, many studies at a regional scale, model the subsurface temperature of a geothermal system at a lithospheric scale using thermal property data combined with geophysical data sets and various modelling techniques (Cloetingh *et al.* 2010; Scheck-Wenderoth & Maystrenko 2013; Scheck-Wenderoth *et al.* 2014; Poulsen *et al.* 2017;

Békési *et al.* 2018; Limberger *et al.* 2018b). These models, which are usually at a national or regional scale rather than resource level, then provide information on suitable areas for further shallow investigations before development of a possible geothermal site development and drilling activities. Modelling the subsurface geotherms allows de-risking drilling costs thus providing a more targeted approach for future investigations.

Closer to Ireland, deep geothermal has been used sporadically for decades in Great Britain (GB) (e.g. Downing & Gray 1985, 1986; Younger *et al.* 2012; Busby 2014; Abesser *et al.* 2020). Since 1979 Southampton has been producing geothermal heat, and combined heat and power, for the civic centre, surrounding businesses and >1000 residential properties (geothermal gradient of 38.5 °C km^{-1}; Downing & Gray 1986; Raine & Reay 2019). More recently, the Eden Geothermal and United Downs projects aim to extract geothermal heat from granitic rocks (Abesser *et al.* 2020; Gan *et al.* 2021; Reinecker *et al.* 2021) with the United Downs project successfully drilling 2 deep geothermal wells to 2.5 and 5 km depth (Reinecker *et al.* 2021), measuring temperatures of ∼180 °C at 5 km depth (Abesser *et al.* 2020). The islands of Ireland and Great Britain have some similarities in their geological histories, including the emplacement of granite sequences and the continuation of lithological units from Ireland across to Scotland (e.g. Dewey & Strachan 2002; Daly 2009; Woodcock & Strachan 2009). The two locations also have comparable surface heat flow values (Mather & Fullea 2019), making it likely that geothermal resources can also be utilized in Ireland.

1.2 Geothermal studies in Ireland

Multiple geothermal studies have been conducted in Ireland including an initial study in 2004 to produce subsurface temperature maps of Ireland's shallow subsurface (Goodman *et al.* 2004; Jones *et al.* 2007). The IRETHERM project (2011–2016) sought to quantify Ireland's geothermal energy potential through integrated lithospheric modelling of geophysical and petrological data (Fullea *et al.* 2014; Jones *et al.* 2014; Farrell *et al.* 2015; Raine & Reay 2019) and modelling magnetotelluric (MT) data with the aim of investigating sedimentary basins with elevated fluid temperatures (Campanyà *et al.* 2015; Delhaye *et al.* 2017, 2019; Vozar *et al.* 2020), identifying fluid circulation pathways of warm springs (Blake *et al.* 2016a; b, 2021) and characterizing Irish granites (Farrell *et al.* 2015; Fritschle *et al.* 2015).

More recently the GEO-URBAN project focused on Vallès (Spain) and the Dublin Basin (Ireland) combining passive seismic, MT and structural geology information to characterize low enthalpy geothermal potential in an urban environment with major fault structures acting as potential fluid pathways (Vozar *et al.* 2020; Maggio *et al.* 2021, 2022). In addition, recent drilling by Geological Survey Ireland (GSI) at the Technical University, Dublin (TUD) Grangegorman campus in 2023, revealed a subsurface temperature of 38.5 °C at 1 km depth (Blake, *Personal Communication 2021*).

Through other projects, subsurface temperature maps have been produced for Ireland from 0 to 5 km depth by CSA for the Sustainable Energy Authority of Ireland (Goodman *et al.* 2004) and the G.O.THERM.3D project (Mather *et al.* 2018; Mather & Fullea 2019) from 2 to 5 km depth. The study of Goodman *et al.* (2004), used temperature data from 117 boreholes from 10 m up to 2500 m deep and interpolated the geothermal gradient using a natural neighbour interpolation to a 1000 m deep model. From 1000 to 5000 m the geothermal gradient was linearly extrapolated due to limited measurements. Near-surface temperature effects in the first tens to hundreds of metres (e.g. solar irradiation) and paleoclimate effects in the first few kilometres, variations in rock thermal properties and deep lithospheric contributions were not considered. The G.O.THERM.3D project modelled crustal layer thickness using receiver functions (Licciardi *et al.* 2014), controlled source seismic data (Landes *et al.* 2005; Hauser *et al.* 2008), crustal magnetic anomalies (Baykiev *et al.* 2018; Mather & Fullea 2019), lithospheric thickness (Fullea *et al.* 2014) and surface heat flow from historic wells in Ireland (Brock & Barton 1984; Brock 1989) and applied paleoclimate corrections (Mather *et al.* 2018; Mather & Fullea 2019), producing temperature maps from 1 to 5 km depth. The data sets and models along with fixed crustal thermal property data (van den Berg *et al.* 2005), were inverted for crustal temperature with models showing geothermal gradients > 20 °C km^{-1} everywhere matching well to global models of geothermal gradient (Limberger *et al.* 2018a). These models predicted exceptionally high temperatures in Northern Ireland beneath basaltic intrusions, which were as high as magmatic high enthalpy geothermal settings. While Goodman *et al.* (2004) and Mather *et al.* (2018) provided valuable information on the subsurface temperatures and geothermal gradient in Ireland, the models are limited by their use of fixed parameters for lithospheric thickness and for the crustal thermal parameters that directly control the subsurface temperatures. Furthermore, the models have no uncertainty associated with them. Estimating uncertainty in the models is crucial to initiate geothermal extraction as it allows the determination of risk associated with drilling and exploitation.

Ongoing projects in Ireland include the De-risking Ireland's Geothermal potential project (DIG) which is an interdisciplinary project from the full island scale to the local scale of the Mallow warm spring region (O'Reilly *et al.* 2021; Kiyan *et al.* 2022). Geophysical surveys including passive seismic and magnetotellurics, in addition to geological field campaigns and hydrochemistry, are being combined to improve our understanding of a known geothermal system (O'Reilly *et al.* 2021; Kiyan *et al.* 2022; Chambers *et al.* 2023). Additionally, GSI's National Geothermal Database is currently being developed and Project InnerSpace (projectinnerspace.org) has a focus on developing geothermal energy usage in Northern Ireland and globally. As part of the DIG project we aim to improve the previous subsurface maps of Ireland (Mather & Fullea 2019 and Goodman *et al.* 2004), and provide associated uncertainty with each point in the model. We have applied indirect geophysical methods with variable thermal property data to model the subsurface temperature and geothermal gradient as 1-D columns and collated to a pseudo-3-D volume. This output model was then compared to direct temperature measurements. These are the first uncertainty maps for subsurface temperature in Ireland, and we also produce new crustal radiogenic heat production, LAB and Moho depth maps.

2 GEOLOGICAL BACKGROUND

The geological evolution of Ireland's crust began in the Precambrian era (Daly 2009) and culminated in the amalgamation of continental and island arc components during the early Palaeozoic (Mitchell 2004; O'Reilly *et al.* 2006; Hauser *et al.* 2008; Graham *et al.* 2009; Woodcock & Strachan 2009). The convergence of the Laurentian and Avalonian continental domains represents the final major event in the formation of Ireland's continental lithosphere forming the supercontinent Laurasia. During the closure of the Iapetus Ocean,

the distribution of radiogenic heat-producing elements in the Irish crust was likely influenced by the process of continental suturing (van den Berg *et al.* 2005; Willmot Noller & Daly 2015; Herrington *et al.* 2018). However, detailed knowledge regarding radiogenic heat production values and their depth distribution across different tectonic terranes remains limited (Lee *et al.* 1987; Mather *et al.* 2018), although new HPR values for lower crustal xenoliths have recently been acquired (Daly, personal communication, 2024).

Transitioning from late orogenic pull-apart basins to mid-late Devonian, extensional sedimentary basins marked a significant change in plate-tectonic configuration (Hauser *et al.* 2008). These basins, particularly the Munster Basin, are a particular focus of recent geothermal projects due to the presence of warm springs (Blake *et al.* 2016a; O'Reilly *et al.* 2021). Central Ireland is predominantly covered by tropical shallow to deep-water Carboniferous limestones, with volcanic rocks locally, deposited in basins in response to marine transgressions. The distribution of carbonate facies is complex and controlled by extensional tectonics, which reactivated major faults in the accreted Caledonian basement. They also influence thermal conductivity values through variations in the mud and silica content (Somerton 1992; Clauser & Huenges 1995; Long *et al.* 2018; Förster *et al.* 2021; English *et al.* 2022).

The Variscan orogeny was most intense in the Munster Basin, where strong tectonic fabrics developed, inverting normal faults into steep-dipping reverse faults with widespread folding, faulting and metamorphism in southern and eastern Ireland (Meere *et al.* 2013; Shannon 2018). Following the Variscan orogeny a period of rifting ensued in the Permian and again in the Early Triassic and was responsible for a number of grabens that developed across Ireland, forming the Kingscourt Outlier in Co. Cavan, and a number of basins across the NE of Ireland (Newtownards Trough, Larne Basin, Lough Neagh Basin, Rathlin Basin, Foyle Basin) (Naylor 1992; Johnston 2004). In northeastern Ireland, Mesozoic to Cenozoic sedimentary rocks are present in extensional basins, offering geothermal reservoir potential in porous sandstones within basins like the Larne Basin (Raine & Reay 2019). The British and Irish Palaeocene Igneous Province was also deposited in northeast Ireland with Palaeocene flood basalt formations (Antrim Lava Group), covering older sedimentary sequences and creating striking landscapes like the Giant's Causeway in Northern Ireland (Cooper 2004; Cooper *et al.* 2008, 2012). Uplift of the lavas and erosion during the Eocene, Alpine compression and development of localized pull-apart basins during the Oligo-Miocene deposited clays and lignite in NE Ireland (Quinn 2006). Significant intrusive activity also occurred at this time emplacing granite complexes such as the Mourne granites.

During the Pleistocene, Ireland experienced several glaciations, with a significant thickness of ice that cooled the crust (Mather *et al.* 2018) and removed much sedimentary cover and sculpted its landscape, leaving behind features like drumlins, eskers and U-shaped valleys.

3 DATA AND METHODS

3.1 Data sets and parameters in the inversion

To produce detailed subsurface temperature maps across Ireland, multiple input data sets across the island of Ireland have been used (Fig. 1, see Supplementary Fig. 1 for the input data sets at the 0.2° x 0.2° resolution used). The best data for the upper crust are direct borehole measurements with calculated SHF and measured TC and lithological information, though these are sparse in Ireland. The temperature maps are produced as a series of points at a lateral resolution of 0.2° x 0.2°, which is the minimum lateral resolution of the surface-wave data produced by Chambers *et al.* (2023). Other data sets such as heat production and thermal conductivity, have a finer resolution which are related to the underlying lithology. However we focus on the coarsest resolution first. In the future this could be improved by having areas of the model with finer resolution for certain parameters while leaving those with more uncertainty as they are. To carry out the inversion each point requires information on the Rayleigh and Love surface waves, elevation, Moho depth, surface heat flow, thermal conductivity and radiogenic heat production in order to determine the lithospheric boundaries and temperature structure detailed above. The input data sets which have been produced by previous studies are described below.

3.1.1 Surface waves

The surface wave data set was created from recent large-scale deployments of broad-band seismometers across Ireland using the permanent Irish National Seismic Network (INSN, www.insn.ie) (INSN 1993; Blake *et al.* 2012) and Great Britain Seismograph Network (Baptie 2018) stations, as well as temporary networks including Ireland Array (Lebedev *et al.* 2012; Lebedev & The Ireland Array Working Group 2022), the Dublin Basin temporary network (Licciardi *et al.* 2014), WaveObs (Möllhoff & Bean 2016), ISLE and ISUME (Landes *et al.* 2004, 2007; Do *et al.* 2006; Wawerzinek *et al.* 2008; O'Donnell *et al.* 2011; Polat *et al.* 2012), the SIM-CRUST project (Piana Agostinetti & Licciardi 2015) and Blacknest (Blacknest 1960). Data from 2010 to 2020 were focused on, in order to maximize coverage across Ireland because the surface waves were computed using pairs of stations present concurrently (Bonadio *et al.* 2021; Chambers *et al.* 2023).

Rayleigh waves: The Rayleigh-wave phase velocity maps are from Bonadio *et al.* (2021). They were computed using data from the networks listed above using the two-station and Automated Multimode Inversion methods (Meier *et al.* 2004; Lebedev *et al.* 2005) and were originally produced on a triangular grid. For each point in the regional grid used in the joint inversion of this study, the closest point in the Rayleigh-wave phase velocity maps was determined and the corresponding phase velocity dispersion curve was extracted, using by-linear interpolation. The Rayleigh-wave phase velocities ranged from 5 to 350 s period, sensitive to crustal and mantle depths, though not every column will have the same period range due to variations in coverage across the island of Ireland. Errors in the data come from instrumental errors including timing errors, response corrections and polarity reversal as well as source effects and systematic errors in the event location and origin times (Bonadio *et al.* 2021). The relative uncertainty assumed for the Rayleigh waves varies with period, with 0.3 per cent at periods $<$ 20 s, 0.1 to 0.3 per cent for 20 to 50 s and 0.3 per cent for periods $>$200 s.

Love waves: The Love-wave dispersion curves and phase velocity maps used in this study are those produced by Chambers *et al.* (2023). These again used data from the seismic networks listed above and are produced in a similar way to the Rayleigh-wave dispersion curves. A dispersion curve was extracted for each point from the dispersion maps at different periods (Fig. 1a). The dispersion curves range from 10 to 250 s and, similarly to the Rayleigh-wave dispersion curves, not every column will have the same period range due to variations in coverage across the island of Ireland. The relative uncertainty assumed for the Love-wave phase velocities also varies with period and is estimated at 0.5 per cent for periods

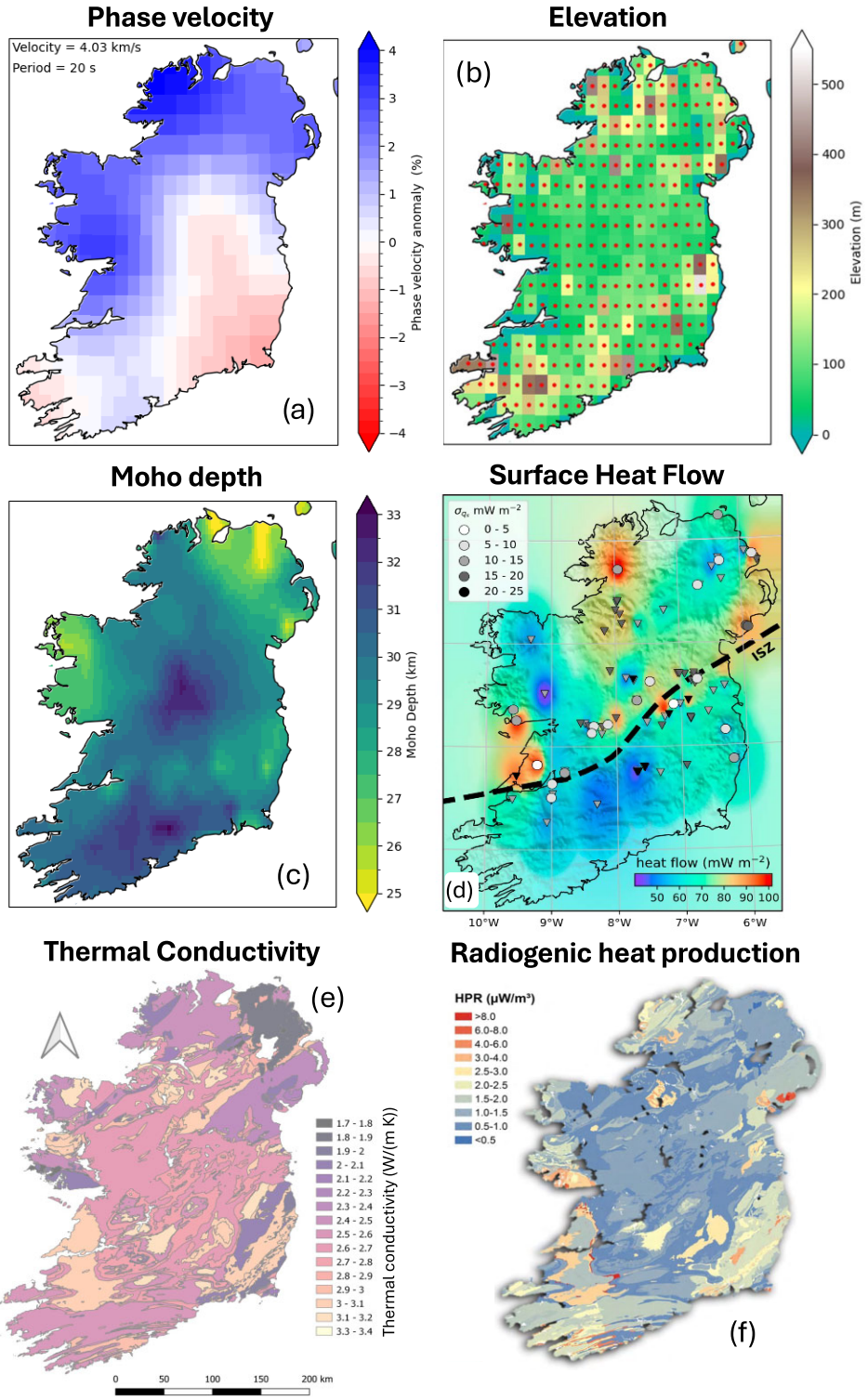

Figure 1. Input data sets used in the joint geophysical–petrological inversion. These include (a) Love- and Rayleigh-wave phase velocities (Bonadio *et al.* 2021; Chambers *et al.* 2023) with Love waves at 20 s shown here (Reference phase velocity is in the upper left corner), (b) Elevation from ETOPO1 (Amante & Eakins 2009), (c) Moho depth, which is a combination of the models of Licciardi *et al.* (2014, 2020) and Bonadio *et al.* (2021, (d) surface heat flow (Mather *et al.* 2018), (e) thermal conductivity (Chambers *et al.* 2023) and (f) surface radiogenic heat production (Willmot Noller & Daly 2015). The points and individual squares on the elevation show the points used in the inversion with a grid spacing of 0.2° x 0.2° which is the same of the Love-wave phase velocity resolution. Actual resolution shown in Supplementary Fig. 1.

<20 s, 0.2 to 0.5 per cent for 20 to 50 s and 0.5 per cent for periods >200 s. This data set covers all of Ireland but has a resolution for the phase velocity maps of 0.2° x 0.2° (Fig. 1b). This is one of the coarser data sets with full lateral coverage across the island of Ireland hence we use this data set as our grid for 1-D columns in the inversion. This results in 703 1-D columns across the island of Ireland.

3.1.2 Elevation

Elevation data were taken from ETOPO1 (Amante & Eakins 2009) (Fig. 1b). For each point at the 0.2° x 0.2° resolution in this study, the average of all points within a 10 km radius was taken and an initial uncertainty ± 10 m was assigned. The uncertainty of this parameter in the inversion is loose with moderate damping to account for the averaging of elevation within each grid square making this value closer to ±50 m.

3.1.3 Moho depth

The input Moho depth is taken from a combination of Bonadio *et al.* (2021) and Licciardi *et al.* (2014), 2020) (Fig. 1c). Bonadio *et al.* (2021) used Rayleigh surface waves to infer the Moho depth while Licciardi *et al.* (2014, 2020) determined Moho depth from receiver functions and reflection and refraction seismic data (Landes *et al.* 2005), which are more direct estimates of Moho depth. Both models are broadly similar in the large-scale structures, though Bonadio *et al.* (2021) have more small -scale variations due to a larger input data set, with most variations < 1 km. Hence, we use an average of the two models in this work. The Moho models were re gridded to the 0.2° x 0.2° used for the inversion, and the average of the two models was taken at each point at 100 m depth increments, which in most instances was the same due to the similarity of the models. This parameter is inverted for in the joint geophysical–petrological inversion but the Moho depth input has an associated uncertainty of ± 2 km accounting for variations in the model (Fig. 1c) and to match the upper end of uncertainty as determined by Licciardi *et al.* (2020).

3.1.4 Surface heat flow (SHF)

Surface heat flow was taken from Mather *et al.* (2018) who interpolated 22 paleoclimate corrected heat flow estimates for the island of Ireland using an inverse distance weighting kernel that accounts for the uncertainty of each point to produce an island-wide map. In this study the values were subsequently regridded from the original map to the 0.2° x 0.2° grid used to parametrize the 1-D columns in the inversion. The map ranges from 45 to 100 mWm^{-2}. SHF is an input data set that the inversion tries to fit within uncertainty. The SHF assigned uncertainty is conservatively ± 5 mWm^{-2} (Fig. 1d) based on the best measurements of Mather *et al.* (2018). However, in the sensitivity analysis we test increasing the uncertainty in these input data to ± 15 mWm^{-2} (compensating for the highest uncertainty in Mather *et al.* 2018) due to the limited number of points used to produce the map.

3.1.5 Thermal properties

Thermal conductivity (TC) values for the upper crust layer were taken from the map in Chambers *et al.* (2023) where a total of 122 TC measurements from different studies (Brock & Barton 1984; Brock 1989; Long *et al.* 2018; Mather *et al.* 2018; ShallowTHERM 2021), varying in location, depth and lithology, were assigned to 19 broad lithological units. Here, an average value from each group of TC values was used for each lithological unit together with an uncertainty estimate based on Chambers *et al.* (2023) (Table 1). Values for TC were taken at each point on the 0.2° x 0.2° grid (Fig. 1e). TC values of 2.75 and 2.5 $W\,m^{-1}\,K^{-1}$ were assigned for the middle and lower crustal layers in the inversion based on continental averages (Artemieva & Mooney 2001; Fullea *et al.* 2014; Limberger *et al.* 2018a) and were kept constant in the inversion within the crust. It should be noted that TC in nature, is dependent on temperature and pressure with TC typically decreasing with increasing depth in the upper crust, and remaining relatively constant in the middle and lower crust. Chambers *et al.* (2023, Supplementary Fig. 2 and Section 3.5) forward modelled a constant crustal TC and a temperature dependent TC in the upper crust. The resulting temperature differences were relatively minor if the constant value is taken as the average of the temperature (and pressure) dependent expression, and would be further moderated by variations in other parameters if a full inversion was performed. What was more crucial was the average value of TC and its match to subsurface lithology. Therefore, a constant crustal TC that is not inverted for, is reasonable to use in the inversion for the crust, which we do here. In the uncertainty analysis, we explored a range of input values for TC in the upper crust, with the ranges dependent on the lithology as defined by the previous TC map from Chambers *et al.* (2023) (Table 1). At mantle depths TC is temperature and pressure dependent (described in Section 3.2.1).

Radiogenic heat production (RHP): Values of RHP from the sedimentary/upper crustal rocks are taken from the map of Willmot Noller & Daly (2015) at each point on the 0.2° x 0.2° grid (Fig. 1f) and assigned to a specific lithology based on the GSI bedrock geology map (Geological Survey Ireland 2020). This is used as a prior value for the average RHP of the whole crust as the inversion can use only one value for crustal RHP (inversion variable) and is updated during each iteration of the inversion. There is minimal damping on this parameter allowing it to freely vary as described in Chambers *et al.* (2023). In future updates to the inversion code, it is intended to assign RHP to individual geological units.

3.2 Joint geophysical–petrological inversion

Here we use a joint geophysical–petrological inversion scheme to invert different data sets for the lithospheric thermochemical structure using a thermodynamic framework (Afonso *et al.* 2008; Fullea *et al.* 2009, 2021; Chambers *et al.* 2023; Lebedev *et al.* 2024). The details on the integrated geophysical–petrological forward modelling and inversion scheme are presented in Afonso *et al.* (2008), Fullea *et al.* (2009) and Fullea *et al.* (2021), respectively. The model is parametrized in terms of mantle temperature and composition and the secondary physical parameters in the mantle (seismic velocities, density) are determined within a self-consistent thermodynamic framework as a function of the primary parameters [e.g. pressure, temperature and bulk mineralogical composition (Connolly 2005)].

3.2.1 The geothermal gradient

The lithospheric geotherm is computed by solving the 1-D heat conduction transfer equation, considering constant and prescribed TC in the upper, middle and lower crust, and a P-T dependent TC in the lithospheric mantle (Afonso *et al.* 2008; Fullea *et al.* 2009, 2021), with the Dirichlet boundary conditions fixed as the temperature at

Table 1. TC ranges for each rock type. The average TC is taken from Chambers *et al.* (2023) where the lithologies are taken from the GSI bedrock viewer and ranges were from previous measurements of TC in Ireland (Geological Survey Ireland 2020).

	Rock type	Average TC ($W\,(m\,K)^{-1}$)	Range TC ($W\,(m\,K)^{-1}$)
1	Palaeozoic basic intermediate volcanics	1.80	1.80 to 2.10
2	Palaeocene basalt	1.90	1.80 to 2.10
3	Cambrian greywacke, slate and quartzite	2.00	1.90 to 2.10
4	Carboniferous volcanics/Devonian volcanics/Ordovician granite/Silurian-Devonian granite and appinite	2.10	1.90 to 2.20
5	Mesoproterozoic gneiss	2.15	2.05 to 2.35
6	Cretaceous chalk flint glauconitic sandstone	2.20	1.60 to 2.80
7	Mesoproterozoic and Paleoproterozoic Annagh Gneiss Complex, granitoid orthogneiss	2.27	2.05 to 2.35
8	Ordovician Silurian marine greywacke and mudstone	2.40	2.10 to 2.80
9	Neoproterozoic metasedimentary rocks (Dalradian)	2.50	2.20 to 2.80
10	Silurian-Devonian conglomerate and mudstone (Old Red Sandstone)/Devonian sandstone and mudstone	2.60	2.20 to 3.40
11	Viséan limestone and calcareous shale	2.70	2.30 to 3.10
12	Jurassic mudstone and limestone	2.75	2.30 to 3.10
13	Tournaisian limestone	2.80	2.30 to 3.10
14	Oligocene clay, sand and lignite	2.90	2.70 to 3.40
15	Permian sandstone conglomerate evaporite/Tournaisian sandstone, mudstone and limestone/Triassic sandstone, mudstone and evaporite	3.00	2.70 to 3.40
16	Ordovician siltstone, sandstone greywacke and conglomerate/Namurian shale, sandstone, siltstone and coal/Silurian marine sandstone, siltstone and conglomerate/Westphalian shale, sandstone, siltstone and coal	3.07	2.60 to 3.40
17	Permian sandstone, conglomerate and evaporite/Tournaisian sandstone, mudstone and limestone/Triassic sandstone mudstone and evaporite	3.10	2.70 to 3.40
18	Viséan sandstone mudstone and evaporite/Silurian deep marine mudstone, greywacke and conglomerate	3.20	2.80 to 3.40
19	Serpentinite and sedimentary mélange	3.40	3.20 to 3.40

the Earth's surface [for Ireland 11 °C; Goodman *et al.* (2004)] and the base of the lithosphere. The LAB is characterized as a thermal boundary here, and separates the lithospheric mantle (with its based pre-defined as the 1300 °C isotherm) and the sublithospheric mantle.

A thermal buffer of variable thickness is defined between the sublithospheric and lithospheric mantle by a superadiabatic gradient. The sublithospheric mantle geotherm (below the thermal buffer) is computed assuming a reference adiabatic gradient and departures from the reference gradient are allowed as required by the data with some bounds. The temperature at the base of the thermal buffer $Z_{\mathrm{buff}} = Z_{\mathrm{LAB}} + \Delta Z_{\mathrm{LAB}}$ is defined as $T_{\mathrm{buff}} = T_a + 100\,^{\circ}\mathrm{C}$. The prior/reference values for T_{sublit1}, T_{sublit2} and T_{bot} for each lithospheric column based on a reference adiabatic gradient ($\gamma_{\mathrm{ref}} = 0.5\,\mathrm{K\ km^{-1}}$) are defined as: $T_{\mathrm{sublit1\_ref}} = T_{\mathrm{buff}} + \gamma_{\mathrm{ref}}((Z_{\mathrm{bot}} - Z_{\mathrm{buff}})/3$, $T_{\mathrm{sublit2\_ref}} = T_{\mathrm{sublit1\_ref}} + \gamma_{\mathrm{ref}}((Z_{\mathrm{bot}} - Z_{\mathrm{buff}})/3$. The sublithospheric temperatures can deviate from their reference values by up to 100 K. The main control for temperature in the inversion is the seismic data (surface wave dispersion curves) which are mostly sensitive to Vs variations and the surface heat flow (Fullea *et al.* 2021). Synthetic surface heat flow values are computed from the temperature gradient at the surface of the model and the crustal TC in each model column.

3.2.2 *Mantle compositional parametrization*

We define the Earth's mantle compositional space within the major oxide system CFMAS (CaO–FeO–MgO–Al_2O_3–SiO_2) which accounts for >98 wt per cent of the Earth's mantle. The major oxides are accommodated in the four main upper-mantle mineral phases: olivine, pyroxenes and an Al-bearing phase. Secondary phases are present but represent on average < 5 per cent of the total assemblage (e.g. Pearson *et al.* 2003). Under the assumption of thermodynamic equilibrium (temperature >500 °C), stable mineral assemblages in the mantle are determined using a Gibbs free energy minimization approach using Perple_X software (Connolly 2005) and the thermodynamically self-consistent data base of Stixrude & Lithgow-Bertelloni (2011). The bulk physical properties of interest in this study (density, seismic velocities) are dependent upon the modal distribution of the main mineral phases and their individual compositions (Connolly & Kerrick 2002; Afonso *et al.* 2008).

3.2.3 *Crustal parametrization*

In contrast to the mantle, large parts of the continental crust are thermodynamically metastable. Therefore, the crust is not defined based on thermodynamic equilibrium in our model: we adopt an *ad hoc* parametrization in terms of the relevant physical properties given the constraining input data sets. The crust is divided into three layers of variable thickness. Within each layer, the model parameters are Vs and density. Crustal *P*-wave velocities are computed from the Vs values from the inversion and fixed Vp/Vs assumed ratios. Moho depth is a free parameter which can vary within the defined uncertainties described in Section 3.1.3. TC is fixed within the crust with the upper crust assigned a value of TC as described in Section 3.1.5, and the middle and lower crust assigned TC values of 2.75 and 2.5 $\mathrm{W\,m^{-1}\,K^{-1}}$, respectively.

3.2.4 *Forward models*

The synthetic phase velocity dispersion curves used in our inversion are computed using a version of the MINEOS modes code (Masters *et al.* 2007, http://geodynamics.org/cig/software/mineos) adapted

Table 2. Model parameters for each crustal layer in the inversion. We include the ranges used for TC and RHP in the upper crust which are based on previous studies (Brock & Barton 1984; Brock 1989; Long *et al.* 2018; Mather *et al.* 2018; ShallowTHERM 2021, Willmot Noller et al 2015). TC and Vp/Vs are fixed in the inversion to the input value whereas we invert for the average RHP, layer thickness, Vs and density. We assign variable weighting depending on confidence in the input parameter with the Moho depth allowed to vary ± 2 km, whereas the upper and middle crustal boundaries can vary ± 5 km. The RHP is loosely damped and is linked to the SHF which is assigned a lower uncertainty as we have more confidence in its value. The density is allowed to vary ± 200 kg m^{-3}. All variations are defined by regularization factors and in some cases (such as RHP) are also tied to the assigned uncertainty in other parameters. For more details see the text. All parameters are variables in the inversion. ∗Range is less than Fig. 1(f), due to averaging of the map to a 0.2 × 0.2° grid.

Layer	Thickness (km)	Vs (km s^{-1})	Density (kg m^{-3})	Vp/Vs	TC W (m K)$^{-1}$	RHP μW m^{-3}	Depth to base of layer (km)
1.Upper crust	10 ± 5	3.52 ± 0.25	2750 ± 200	1.75	1.7–3.4	0.5–4.0∗	10
2. Middle crust	10 ± 5	3.71 ± 0.25	2900 ± 200	1.75	2.75	0.7	20
3. Lower crust	10 ± 2	3.94 ± 0.25	3050 ± 200	1.75	2.5	0.4	24–34

for the travelling wave decomposition, appropriate for surface waves (Nolet 2008). Below 660 km depth, the reference model AK135 is assumed for all the relevant parameters (Kennett *et al.* 1995). In the mantle transition zone (410 km < depth < 660 km) only the density, Vp and attenuation parameters are taken from AK135, with the *S*-wave velocities at the 410 and 660 km discontinuities being inversion variables inverted for.

The predicted surface elevation is computed by integrating the crustal and lithospheric mantle densities assuming local isostasy, that is the pressure at the base of every vertical lithospheric column be the same when integrated down to a certain depth, known as the compensation level. The density integration is only over the lithosphere and we do not explicitly include sublithospheric loads as part of the isostatic equilibrium. Predicted surface heat flow values are computed from the surface temperature gradient and thermal conductivity.

3.2.5 *Inversion scheme*

The data sets that we invert for are mostly sensitive to temperature variations which can be modelled in 1-D and consequently there is no explicit lateral regularization. Modelling in 1-D also speeds up the inversion scheme (see Section 5.5 for limitations on the 1-D assumption). The laterally independent nature of the physical forward problems allows for parallelization of the inversion, where different lithospheric columns can be treated separately. The data vector, $d_{\rm obs}$, is given by: $d_{\rm obs} = [E,\ {\rm SHF}, \phi_i^{\rm Ray}, \phi_j^{\rm Love}]^t\ i = 1,\ N^{\rm Ray}, j = 1, N^{\rm Love}$, where $N^{\rm Ray}$ and $N^{\rm Love}$ are the number of periods for Rayleigh and Love waves for each dispersion curve, respectively, E is the surface elevation and SHF is the surface heat flow (Fullea *et al.* 2021).

We invert the Rayleigh and Love surface-wave dispersion curves along with SHF and surface elevation which are weighted based on the uncertainty in each measurement. We follow the procedure of Chambers *et al.* (2023) which is similar to Fullea *et al.* (2021) and references therein, with a modification: a vertical gradient damping is applied to radial anisotropy when inverting for shear-velocity to allow velocity to change more smoothly with depth. For density we invert for the upper, middle and lower crustal density using the reference parameters in Table 2. The output from the inversion includes the lithospheric geotherm, lithospheric thickness and Moho depth, as well as crustal structure (seismic velocity, density and radiogenic heat production), and radial seismic anisotropy.

The model vector, m includes crust and mantle inversion variables:

$$m = [\rho_{\rm i}^{\rm c}, {\rm Vs}_{\rm i}^{\rm c}, {\rm H}^{\rm c}, {\rm Z}_{\rm i}^{\rm c}, {\rm Z}_{\rm LAB}, {\rm T}_{\rm sublit1}, {\rm T}_{\rm sublit2}, {\rm T}_{\rm bot}, {\rm C}_{\rm lit}, {\rm C}_{\rm sublit}, \Delta {\rm Z}_{\rm LAB}, {\rm Vs}_{410}, {\rm Vs}_{660}, {\rm Anis}_{\rm k}]^{\rm t},\ {\rm i} = 1, 3\ {\rm k} = 1, 13,$$

where $\rho_{\rm i}^{\rm c}$ and ${\rm Vs}_{\rm i}^{\rm c}$ are the crustal densities and *S*-wave velocities for a three-layered crust, ${\rm H}^{\rm c}$ is the average crustal radiogenic heat production (RHP), ${\rm Z}_{\rm i}^{\rm c}$ is the depth of the base of each crustal layer; ${\rm Z}_{\rm LAB}$ is the depth of the LAB, ${\rm T}_{\rm sublit1}$, ${\rm T}_{\rm sublit2}$, ${\rm T}_{\rm bot}$ are the sublithospheric temperatures at depths ${\rm Z}_{\rm buff} + \frac{{\rm Z}_{\rm bot} - {\rm Z}_{\rm buff}}{3}$, ${\rm Z}_{\rm buff} + \frac{2({\rm Z}_{\rm bot} - {\rm Z}_{\rm buff})}{3}$ and ${\rm Z}_{\rm bot}$ respectively (${\rm Z}_{\rm bot} = 400$ km, ${\rm Z}_{\rm buff} = {\rm Z}_{\rm LAB} + \Delta {\rm Z}_{\rm LAB}$), $\Delta {\rm Z}_{\rm LAB}$is the thermal thickness of the lithospheric buffer, ${\rm Vs}_{410}$ and ${\rm Vs}_{660}$ are the *S*-wave velocities at the 410 and 660 km mantle transition discontinuities, and ${\rm Anis}_{\rm k}$ are the radial anisotropy values at the three crustal layers and at 56, 80, 110, 150, 200, 260, 330, 400, 410 and 660 km depths within the mantle, respectively and C_{lit}, $C_{\rm sublit}$ are the bulk amounts of Al_2O_3 in the lithosphere and sublithosphere, respectively. Following Fullea *et al.* (2021) here we only invert for Al_2O_3 as the mantle compositional parameter, with correlated values of CaO–MgO based on global petrological data bases as described in Afonso *et al.* (2013).

The misfit function is defined as:

$$S(m) = [g(m) - d_{\rm obs}]^t C_D^{-1} [g(m) - d_{\rm obs}]^t + [m - m_{\rm ref}]^t C_M^{-1} [m - m_{\rm ref}]$$

from Fullea *et al.* (2021), where *g(m)* is the nonlinear forward operator that maps the model vector (m) into the observational space ($d_{\rm obs}$), in this case the joint geophysical–petrological modelling approach. The first term of S(m) is a quadratic, corresponding to the square of the weighted data misfit L2-norm, including data uncertainties. C_D^{-1} and C_M^{-1} represent the inverse observational and model covariance matrices, respectively, here assumed to be diagonal. The diagonal elements of C_D are defined by the (squared) data uncertainties plus the model uncertainties, and are used to weight the contribution of the different data sets in $d_{\rm obs}$. The second term of S(m) regularizes the inversion problem. C_M is a diagonal matrix of squared weighting factors for the respective elements of the reference (and regularizing) model vector, $m_{\rm ref}$. For the crustal inversion parameters (velocity, density and thickness), radial anisotropy, lithospheric thickness and mantle composition the regularization term is explicit. The geotherm represents an additional regularization term: thermal steady state in the lithosphere (heat conduction domain) and adiabatic gradient(s) in the sublithosphere (heat convection domain). The regularization term prevents the inversion from falling into non-physical solutions outside of the domain of the joint geophysical–petrological forward problem solver (Fullea *et al.* 2021). Finding an optimal balance between data fit and regularization is a complex, problem-dependent task that has to be adapted to the particular inversion problem one is dealing with.

The inversion is performed on 1-D columns (703 in total) which are distributed in a 0.2 × 0.2° grid across the island of Ireland (Fig. 1b), each reaching from the surface to 660 km depth, in contrast to Chambers *et al.* (2023) who inverted six columns with reliable geophysical, petrophysical and thermal input data. We assign

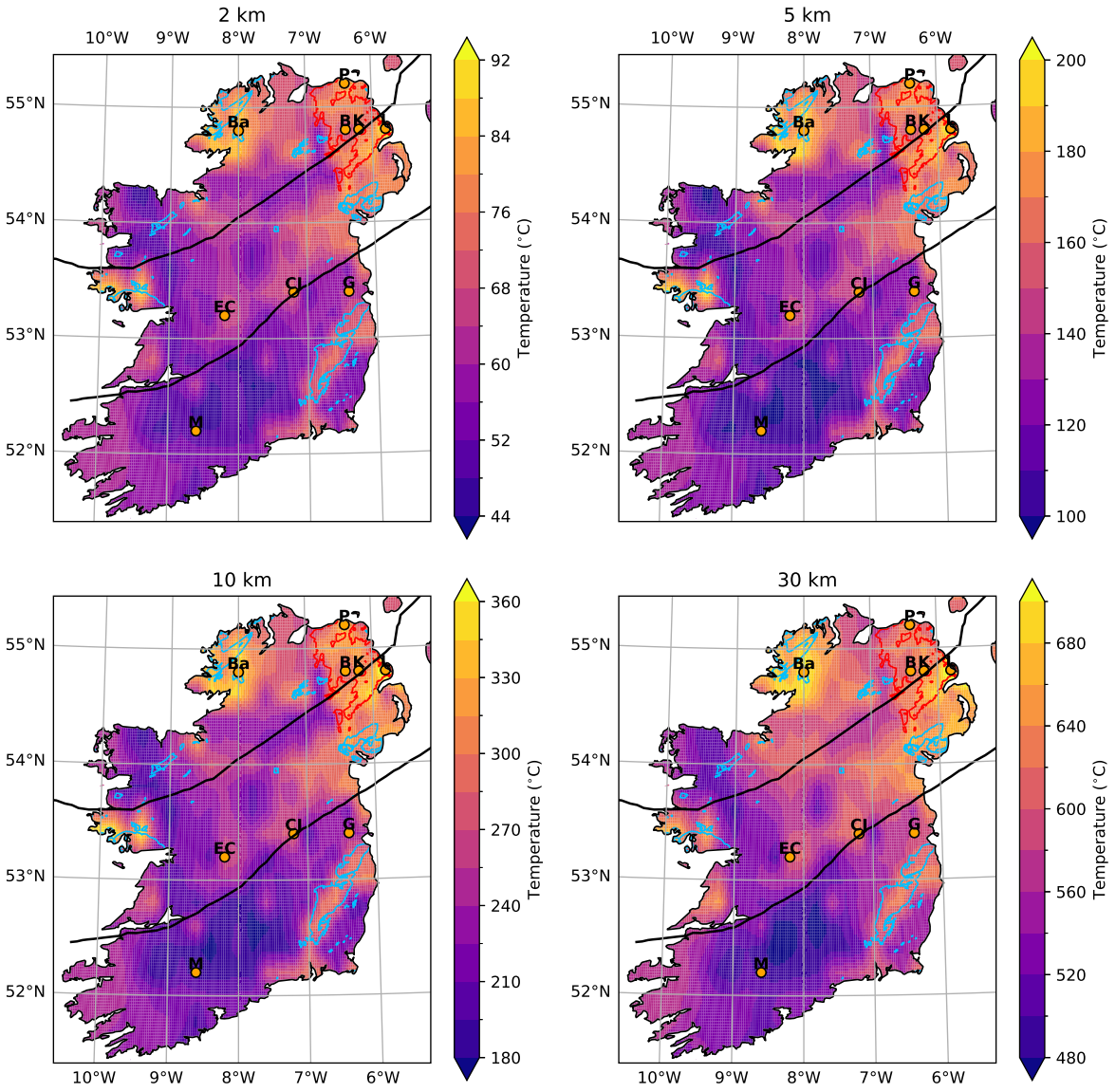

Figure 2. Subsurface temperature maps of the island of Ireland at 2, 5, 10 and 30 km depth. Data have been cropped to the coastline and smoothed. The Iapetus Suture Zone marked by thick black lines, Basaltic bedrock as red polygons and granites by light blue line [Bedrock units taken from the GSI bedrock geology viewer (Geological Survey Ireland 2020)]. Orange points are locations referred to in the text and 1-D columns shown in Fig. 4. Acronyms are: B—Ballymacilroy, Ba—Barnesmore Donegal, CJ—Castle Jordan, EC—Eyres Court, G—Grangegorman, K—Kells (NI), L—Larne, M—Mallow, P—Portmore.

reference values with variable damping coefficients to regularize our inversion. For the three layers of the crust we assign an averaged reference shear velocity, density and thickness for each layer calculated from the reference seismic model BL21 in Ireland (Bonadio *et al.* 2021) and specify a Vp/Vs value for each layer based on seismic refraction studies (Hauser *et al.* 2008) which are shown in Table 2. The damping parameters for density, crustal thickness, shear velocity and radial anisotropy were tested and allowed to vary according to the confidence in each value. Previous studies of Moho depth find results with uncertainties of ±2 km (Licciardi *et al.* 2014, 2020); Bonadio *et al.* (2021) suggesting strong damping can be imposed. In contrast, crustal velocity and density are less well-constrained beneath Ireland and Britain, so we allow these values more freedom to ensure a good misfit but not unreasonable oscillations. Similarly, TC was assigned to each of the three layers in the crust: the TC map of Chambers *et al.* (2023) (Fig. 1a) for the upper crust, 2.75 and 2.5 W m^{-1} K^{-1} for the middle and lower crust, respectively.

4 RESULTS

703 1-D columns of Ireland's subsurface were inverted and collated to make a 3-D temperature model which was interpolated to 1 km spacing in depth (interpolated to 10 m intervals for the depth to the 30 °C, 60 °C and 90 °C isotherms). The output 1-D temperature columns extend from the topographic surface to 660 km depth but the focus for this paper is from the surface (elevation/topographic height) to the base of the lithosphere (LAB) (Fig. 2 and Supplementary Fig. 2). For presentation purposes we smooth the models, but the original grid spacing can be seen in Fig. 1(b) and Supplementary Fig. 1.

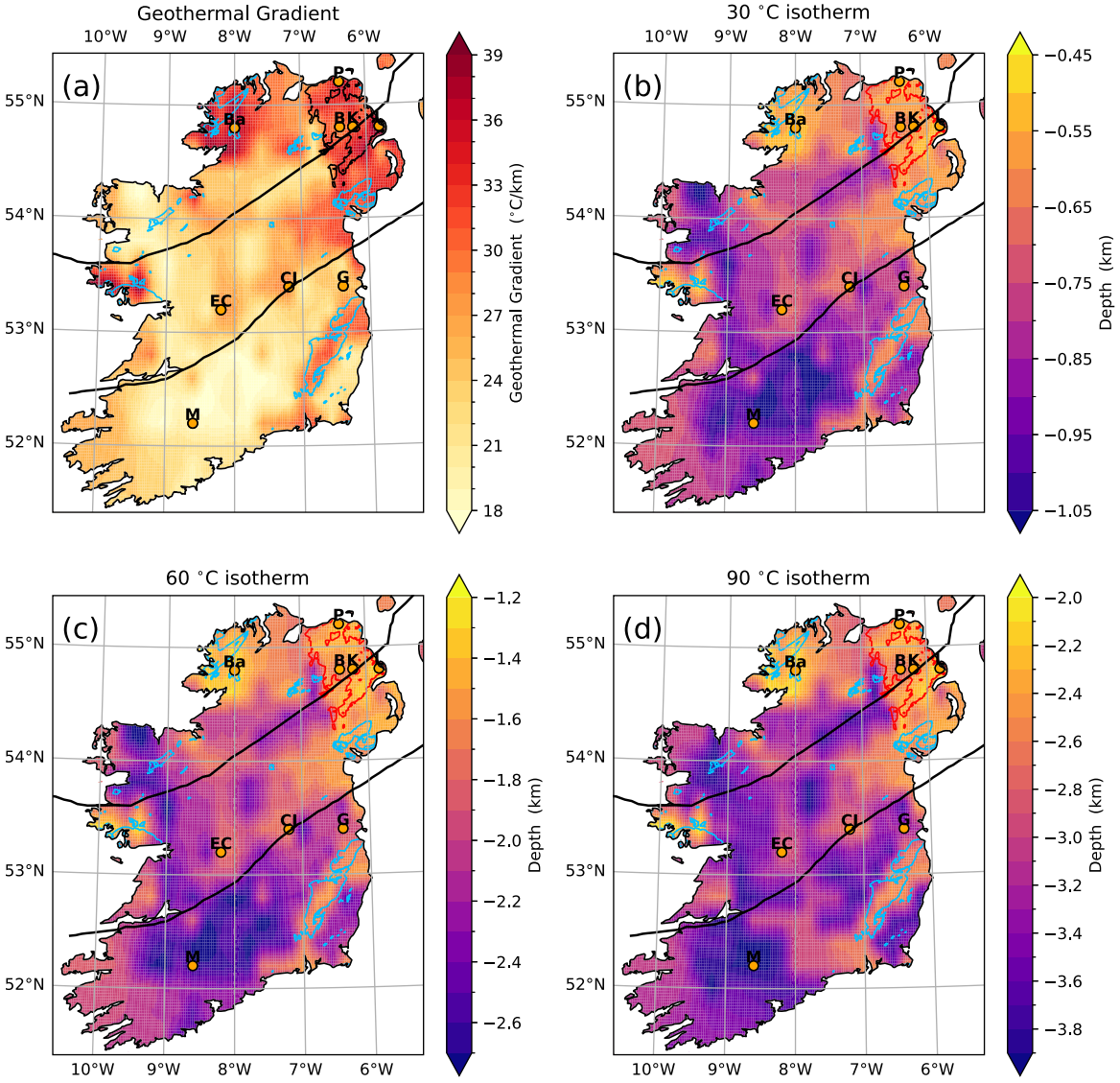

Figure 3. Geothermal Gradient map (a) and depth to the 30 °C, 60 °C and 90 °C (b–d) isotherms. Note variable colour scales. See Fig. 2 for symbol descriptions.

The new subsurface temperature maps (Fig. 2) range from < 50 °C to 90 °C at 2 km depth for all of the island of Ireland. The models suggest temperatures are warmest in the north and east of the island (75 °C to 90 °C at 2 km depth) and in areas with surface granite exposure (>85 °C for the Co. Donegal and Galway granites, and 75 °C to 80 °C beneath the Leinster and Mourne granites at 2 km depth). Temperatures are cooler in the south and in the Midlands ranging from < 50 °C to ∼70 °C, at 2 km depth.

The geothermal gradient (Fig. 3a) is computed from the modelled temperatures at 1 and 2 km depth and the upper crustal TC value assigned based on lithology. We only average the first km as the gradient for the model is broadly linear for the first 10 km as shown in Fig. 4 and Supplementary Fig. 3. This is due to limitations in the parametrization of the model as having a 3-layered crust rather than variations for each lithological unit. The geothermal gradient ranges from < 20 °C km^{-1} in the south and Midlands, before increasing to > 30 °C km^{-1} for the Leinster granite and east coast of Ireland. The geothermal gradient increases northwards to 35 °C km^{-1} beneath much of Northern Ireland, reaching a maximum of ∼40 °C km^{-1} beneath the Donegal and Galway granites (Fig. 3a). In addition, the depths to the 30 °C, 60 °C and 90 °C isotherms were extracted from the temperature volume (Figs 3b–d). These show a similar pattern to the temperature maps with areas of warmer temperature having shallower depths to the isotherms and cooler regions being deeper and having the coolest geothermal gradient, as expected. The depth to the 30 °C isotherm ranges from 450 m to 1.1 km depth whereas the 90 °C is located between 2 and 3.8 km depth (Fig. 3).

The output RHP ranges from 0.5 to 2.0 μW m^{-3} (Fig. 5) with the highest values in the northwest beneath the Donegal granites, and in the Iapetus Suture Zone, extending from county Clare to the Mourne granites. The lowest RHP values are in Co. Galway and the south of the island of Ireland. Moderate RHP values are found beneath the Antrim basalt sequences (∼1.0 μW m^{-3}). The area of the Leinster granites has higher RHP than the surrounding rocks by +0.2 μW m^{-3}.

As an independent comparison, (Chambers *et al.* 2023, figs 12 and 13) compared modelled temperature from the integrated inversion with measurements in six boreholes, finding that all temperature values were reproduced within ± 2 °C at 2 km depth for RHP and

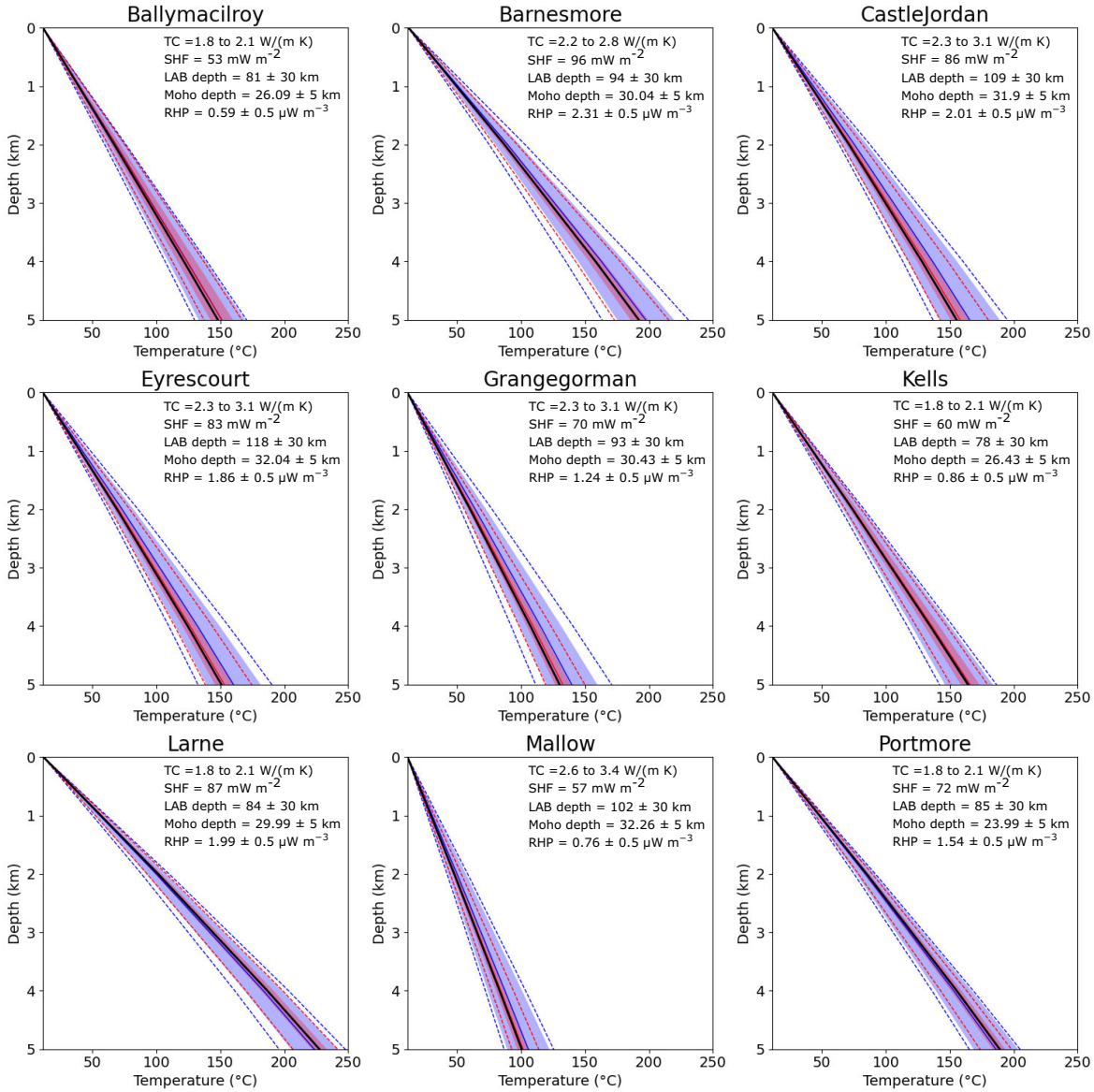

Figure 4. Uncertainty analysis for nine columns with the best original input data from 0 to 5 km depth. The best temperature is plotted as a thick black line and the green dashed lines show the minimum and maximum temperature for 1 fixed input parameter/variable at a time, with the mean indicated by the thick green line and the shaded region the standard deviation either side of the mean. The blue lines are the same as the green lines but for all the key input parameter/variable fixed within plausible ranges, see the text for further details. The best temperature always plots within both standard deviations. The RMS and standard deviation are similar to one another so only standard deviation is shown here.

TC ranges based on the local bedrock geology for the upper crust, providing confidence in the models. This is also within the RMS value computed described in Section 5.1.3 and as shown in Fig. 6. Another comparison between our model and the recently drilled Tallaght GT1 well, found our model suggested a depth of 900 m to the 30 °C isotherm (model interpolated to 100 m depth increments) with the measured value at 749 m for the 30 °C isotherm (*Personal communication GSI and GeoServ*). The direct temperature measurement was taken within the first week after drilling and was not corrected to account for paleoclimate effects which could vary by up to 3 °C (Mather *et al.* 2018) to add to the uncertainty and limitations of our modelling. Given no prior petrophysical information was used in the inversion at this location, the closeness of fit, though relative, shows this procedure gives a good starting point for further local scale studies to refine the geothermal gradient.

As a by-product of the thermal modelling we have derived new maps for the depth to the Moho and LAB (Figs 7a and b). The new Moho model ranges from 25 to 33 km, with thicker crust in southern and central Ireland at 30 to 33 km thick, and thinner crust in counties Galway, Mayo, NE Ireland and eastern Co. Donegal (25 to 29 km thick). The crustal thickness ranges from $<$26 km in the northeast of the island, increasing to $>$32 km in central Ireland with average values of 29.5 km for the island of Ireland (Fig. 7a). The obtained LAB depth (Fig. 7b) shows similarities to the Moho depth map with the thickest lithosphere in

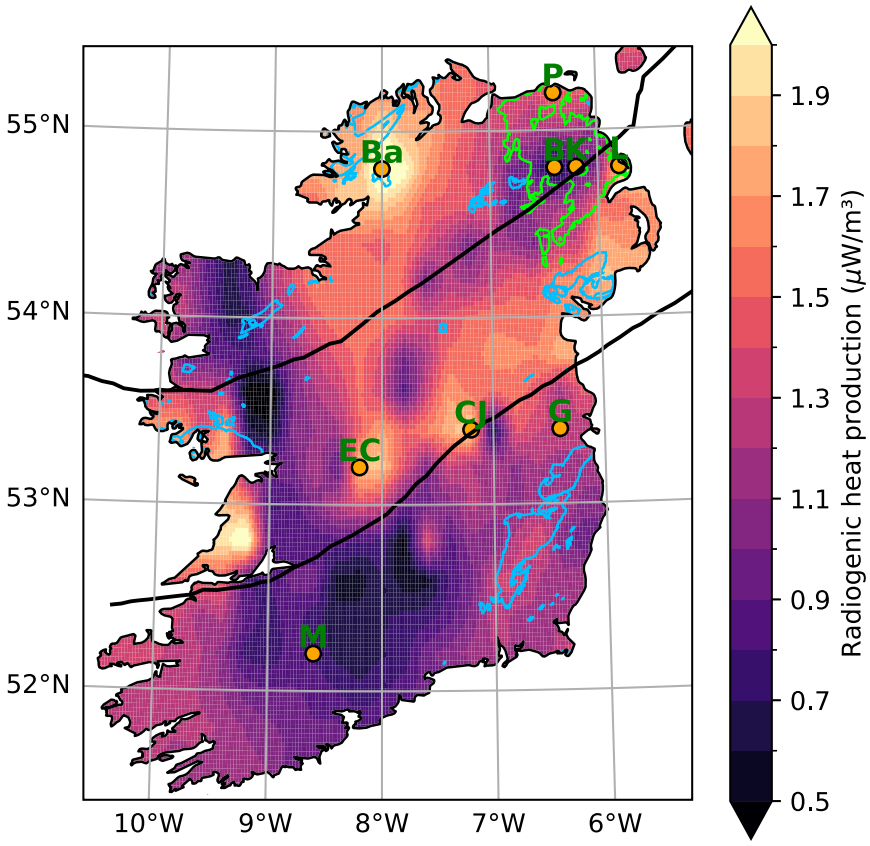

Figure 5. Radiogenic heat production (RHP) map derived from the inversion results for Ireland. The highest RHP is beneath areas with thicker crust which may reflect more felsic crustal compositions or are granitic regions. In contrast the lowest RHP values are within the Iapetus Suture Zone and the south of Ireland where we also have lower SHF and cooler temperatures. See Fig. 2 for symbol descriptions.

central Ireland (112 km) and southwest Ireland (108 km), thinning to 76 km in northeast and average values of ∼94 km thick. Broadly both the Moho and LAB maps thin from southwest to northeast. Both the LAB and Moho depth maps show a clear change between north and south of the Iapetus Suture Zone with thicker crust and lithosphere south of this boundary and thinner to the north.

5 UNCERTAINTY ANALYSIS AND LIMITATIONS

5.1 Uncertainty analysis

We carried our two uncertainty tests in order to determine the final temperature uncertainty at every 1-D point across the island of Ireland. This is the uncertainty based on the pseudo 3-D temperature model and is a lower bound of the real uncertainty. The approach followed here to estimate the inversion model uncertainties is based on the idea of sampling projections of the multidimensional model space (e.g. Bartzsch *et al.* 2011; Lebedev *et al.* 2013). In this way we construct a multidimensional grid for the key inversion variables/parameters and run inversions for every fixed combination of values with the rest of the model variables free to vary and evaluate the misfit function.

The resulting multidimensional misfit surface is the projection of the total model space onto the chosen key variables/parameters subspace containing information on the resolution and possible trade-offs between them. The key variables/parameters controlling the temperature distribution analysed in this work are TC (an input parameter) and inversion variables RHP, Moho depth and LAB depth.

The two uncertainty analyses were performed on nine representative columns to save on computational costs in this exploratory phase. The nine columns were chosen as columns with the most reliable input data, locations with direct temperature measurements and/or in areas of interest such as granitic regions or Mallow, an area of geothermal interest where the warm springs are currently exploited. Four of these overlap with the columns used for testing in Chambers *et al.* (2023) (Mallow, Eyres Court, Barnesmore/Donegal, Kells/Northeast Ireland) and the remaining five are locations with borehole temperature measurements which were used as comparisons to direct temperature measurements in Chambers *et al.* (2023) (temperature profile lengths for: Grangegorman 0.997, Ballymacilroy 0.85 km, Larne 2 km, Portmore 1.482 km and Castle Jordan 0.79 km. Note, the total borehole length for each location exceeds 1 km). For test 1 the key inversion variables/parameters were all fixed, whereas in test 2 only one of the key inversion variables/parameters was fixed in the inversion, to allow trade-off with the other variables. The values for the key inversion variables/parameters were selected as ranges suitable for Ireland. Each variable interval was split into discrete equally spaced points (Table 3) for the uncertainty analysis.

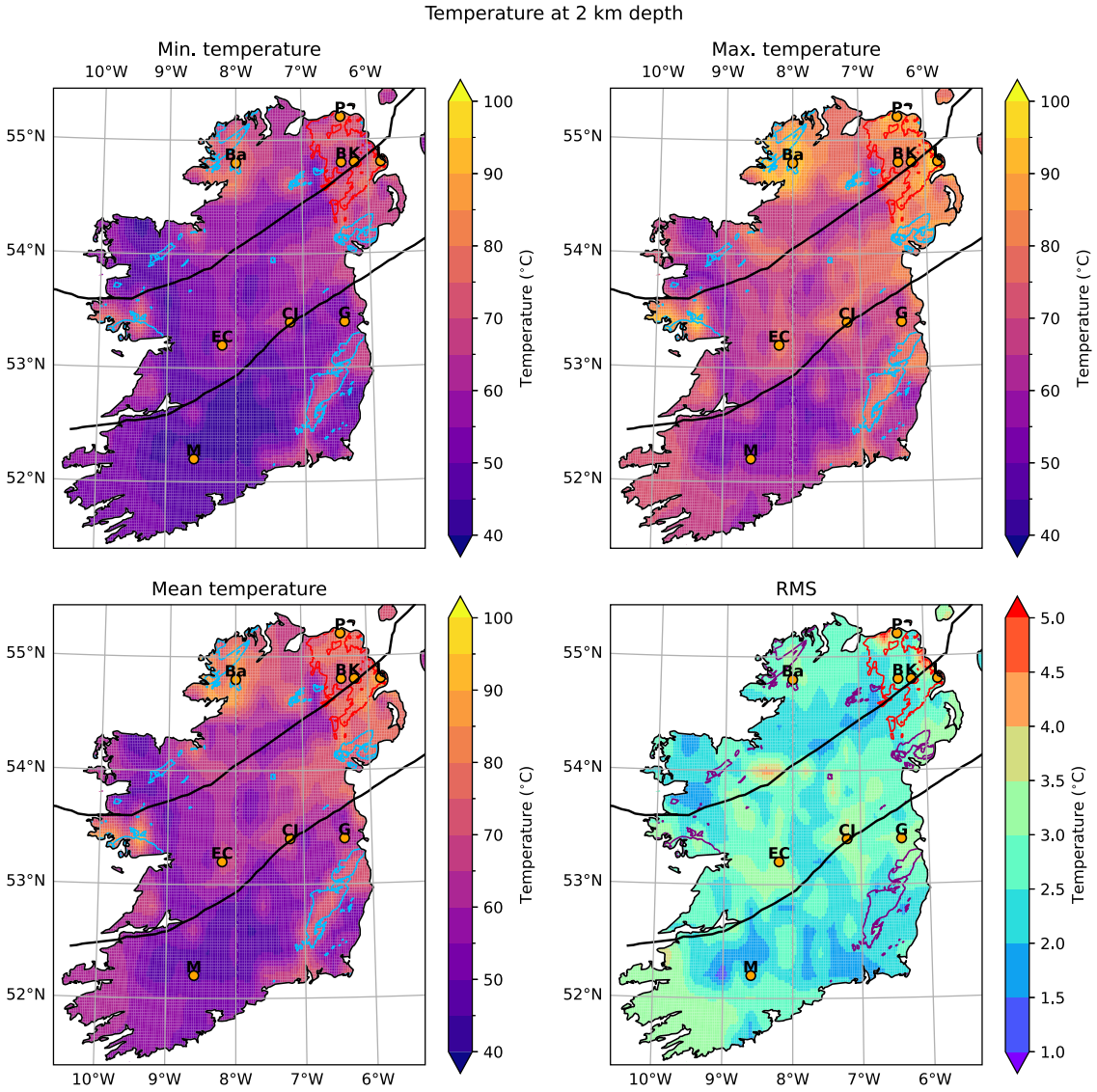

Figure 6. Uncertainty analysis for every point at 2 km depth. Minimum, maximum and the mean temperature for all possible input parameters are plotted. Uncertainty for the 2 km temperature slice is shown in the bottom right panel. See Fig. 2 for symbol descriptions.

5.1.1 1-D uncertainty analysis on nine columns—test 1: keeping all four key parameters/variables fixed within plausible ranges

To determine uncertainty for the final best temperature model, an intensive analysis was carried out on the nine representative columns. TC (an input parameter) and key inversion variables controlling the temperature distribution (RHP, Moho depth and LAB depth) (Table 1 and Table 3) were fixed to a range of plausible values with all other parameters being free to vary in the inversion, in order to estimate their uncertainty and the overall trade-off between the parameters. The ranges for each parameter/variable used in the uncertainty analysis are summarized in Table 3. Thermal conductivity was varied in plausible ranges (Table 1) for the expected bedrock geology at each point based on the TC map of Chambers *et al.* (2023) and the GSI bedrock viewer (Geological Survey Ireland 2020). This results in the maximum temperature variation of the output model (Fig. 4, blue lines and Supplementary Fig. 3), suggesting TC is one of the main controls on temperature in the upper crust. The variations were large and resulted in many unrealistic models (e.g. very high SHF but negligible RHP and a thick Moho) with high variability, however the mean was similar to the best model.

5.1.2 1-D uncertainty analysis on nine columns—test 2: keeping just one of the key parameters/variables fixed

While the selected key parameters/variables are the ones that most affect our crustal temperatures in the inversion, they are also correlated with one another. Therefore, fixing all key parameters/variables independently of each other will likely select combinations of output models that do not make sense physically, but were necessary to be systematic in the analysis. Varying all key parameters/variables together within sensible ranges is also computationally expensive so test 2 was run where only one parameter/variable was kept fixed at a time and changed for each inversion

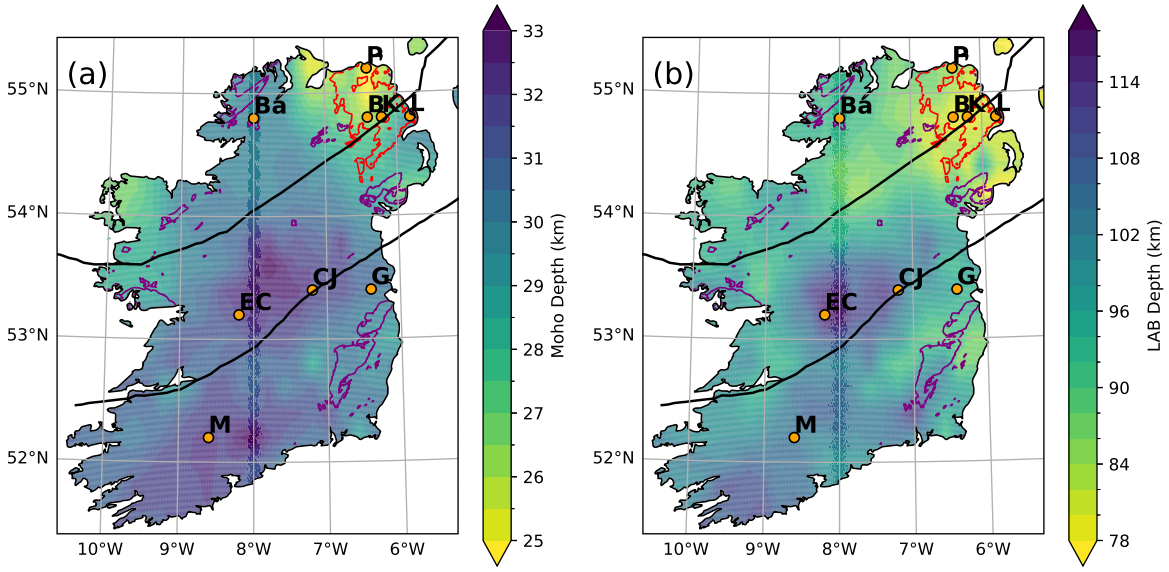

Figure 7. (a) Moho and (b) Lithosphere Asthenosphere Boundary (LAB) maps of Ireland. The thickest crust and lithosphere is in central and southern Ireland whereas thinner crust and a shallower LAB are beneath Northern Ireland, the north of the island of Ireland and at Mayo and Galway on the west coast. See Fig. 2 for symbol descriptions.

Table 3. Parameter/variable ranges used for the testing of the uncertainty in the temperature models. For parameters with ±, each point of the best model was run within this range. ∗ Thermal conductivity was varied within specific lithological ranges as listed in Table 1 with 0.1 W (m K)$^{-1}$ increments.

Parameter	TC (W (m K)$^{-1}$)	RHP (μW m^{-3})	Moho depth (km)	LAB depth (km)
Range	∗	± 0.5 (0.1 μW m^{-3} intervals)	± 5 (1 km intervals)	± 30 (5 km intervals)

while the rest were inverted for. Test 2 is considerably less computationally intensive compared to the test 1 in the uncertainty analysis, at the price of sampling fewer regions of the total model space. The results indicate that the minimum and maximum temperature range is smaller at lithospheric depths when only one key input parameter/variable is kept fixed at a time for each inversion and allowed to change between inversions within sensible ranges, as expected (Fig. 4, red lines).

Once all possible inversions had been run, the overall uncertainty of the accepted models is then calculated as the root mean square (RMS) of the difference between the acceptable output temperature models T_m, and the best temperature model T_i for an individual column:

$$\mathrm{RMS} = \sqrt{\overline{(T_i - T_m)^2}}.$$

We inspected the data misfit for the first and the second uncertainty tests in the nine selected columns [see Section 3.2.5 for the definition of the misfit and further information can be found in Fullea *et al.* (2021), Section 5.1]. The spread of the data misfit was analysed, and the misfit ratio (misfit new model/misfit best temperature model) were compared. Based on the distribution of the output models, a misfit ratio of 1.05 was chosen. This value was chosen as it kept a balance between having a low RMS in the accepted models and keeping sufficient models to assess uncertainty, while removing those that are unrealistic (Supplementary Figs 4 and 5). Both tests showed the RMS uncertainty stabilizing beyond a certain misfit, though this was always a higher RMS for uncertainty test 1, with lower RMS observed for uncertainty test 2. For test 2, we selected the misfit ratio as the inflection point for the majority of columns which was 1.05 (Supplementary Fig. 4). The RMS increases at lower misfit thresholds for test 2 due to insufficient number of models included in the analysis. The misfit in the Love and Rayleigh waves was also plotted for test 1 (Supplementary Fig. 5a) and test 2 (Supplementary Fig. 5b) for a range of misfit ratios, with 1.05 a good balance between sufficient models and removing extreme misfit values.

The RMS and standard deviation (STD) are smaller for test 1 (Fig. 4 and Supplementary Fig. 2). However, the best model and the mean models all fall within the STD bands for both tests. We conclude that running uncertainty tests where only one key parameter/variable is modified at a time, is representative for the full inversion and is sufficient to produce reliable uncertainty plots at every point in our model for the 0.2° x 0.2° grid (Fig. 6 and Fig. 8).

5.1.3 Uncertainty analysis for all 1-D columns

Finally we adopt the uncertainty analysis strategy of test 2, on all 703 1-D columns to make a pseudo 3-D uncertainty volume at every point in the 0.2° x 0.2° grid (Table 1 and Table 3). Points that were in the sea were removed as the input data sets cover the land area only. Additionally, columns that were predominantly offshore were removed as our parametrization of the inversion requires onshore crust with positive elevation. Models with a misfit > 5 per cent larger than the original best model were removed (Fig. 8).

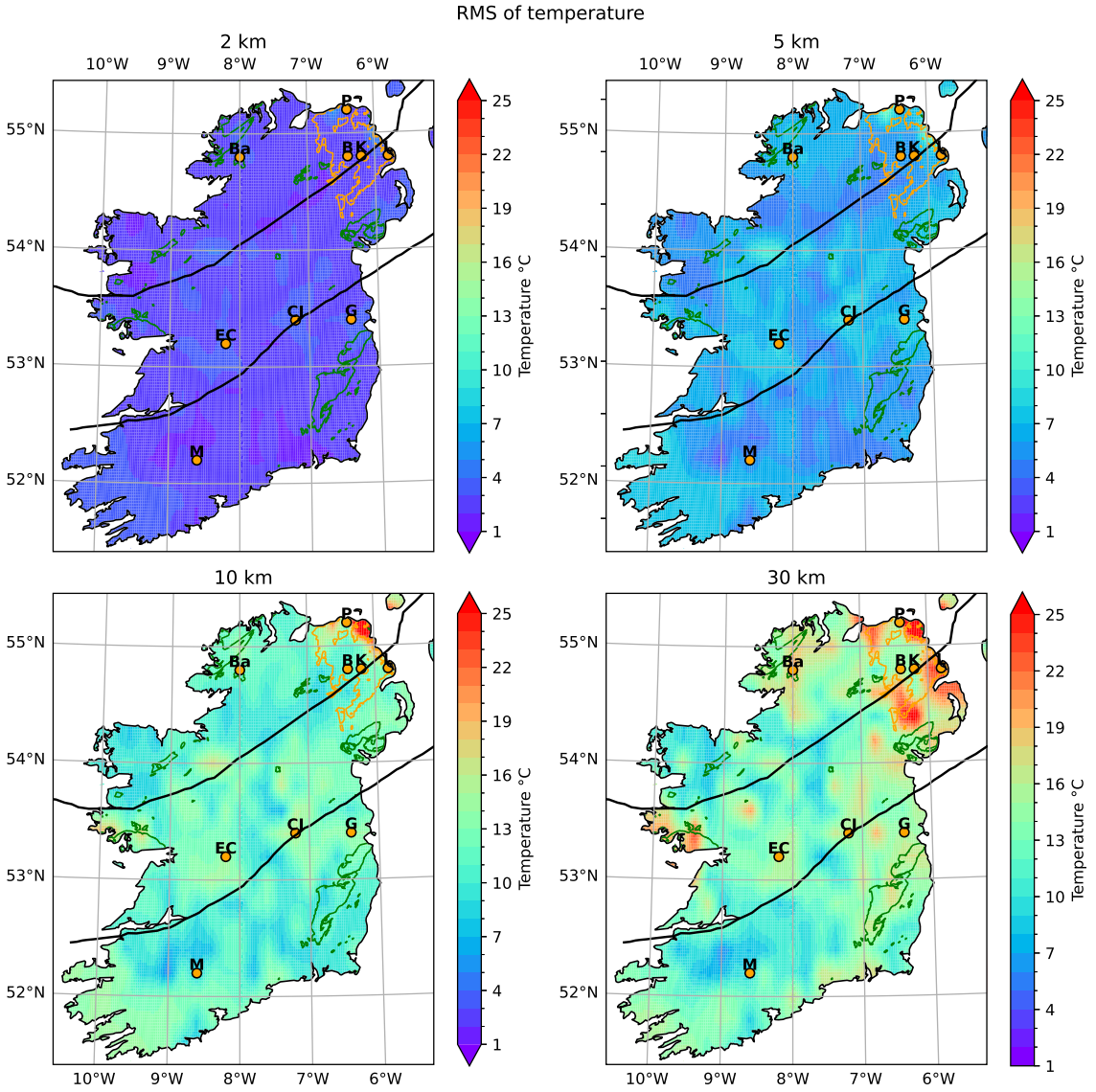

Figure 8. Uncertainty maps showing the temperature variation with increasing depth for our model. Depth slices at 2, 5, 10 and 30 km are shown. See Fig. 2 for symbol descriptions.

5.2 Sensitivity analysis: input SHF

The SHF map contains, in places, high uncertainty from interpolation between limited data points to make the final input map in the 0.2° x 0.2° grid (Mather *et al.* 2018). In addition, SHF measurements can in some cases be affected by local perturbing processes not accounted for in our model parametrization such as thermal disequilibrium due to drilling. Given the variation in uncertainty for the input SHF values, we also tested the sensitivity of the model when the input SHF is modified.

First, we tested the case of high uncertainty. We increased the uncertainty in the SHF to ±15 mW m^{-2}, allowing the inversion more freedom to fit the SHF from the original ±5 mW m^{-2} (green line in Fig. 9). The second test was to fix the SHF to extreme values within the uncertainty range and force the inversion to fit the value. The purpose of this test is to assess the effect of varying the input SHF and forcing the inversion to match that value. Three inversions were then run on each of the nine columns: (1) with the expected best SHF value (orange line) and (2) & (3) ±15 mW m^{-2} difference from this value (blue and red lines)(Fig. 9). The tests for extreme SHF and very low uncertainty (i.e. forcing the inversion to match the input SHF value) produced significantly higher misfit values and modified the resulting geotherms significantly (Fig. 9 and Supplementary Fig. 6). These values are higher than the variations we expect from our model and highlight the importance of using the best input data possible and providing a realistic uncertainty value for any input datum. When using a high uncertainty for the input data, the temperature model converged to a similar result as the best model and also within the modelled temperature uncertainty, determined by the uncertainty analysis described above. Furthermore, if the input SHF is wrong or contains perturbations not accounted for in the thermal modelling and the inversion is forced to match that value, then the output results are unrealistic with a poorer match to the seismic data.

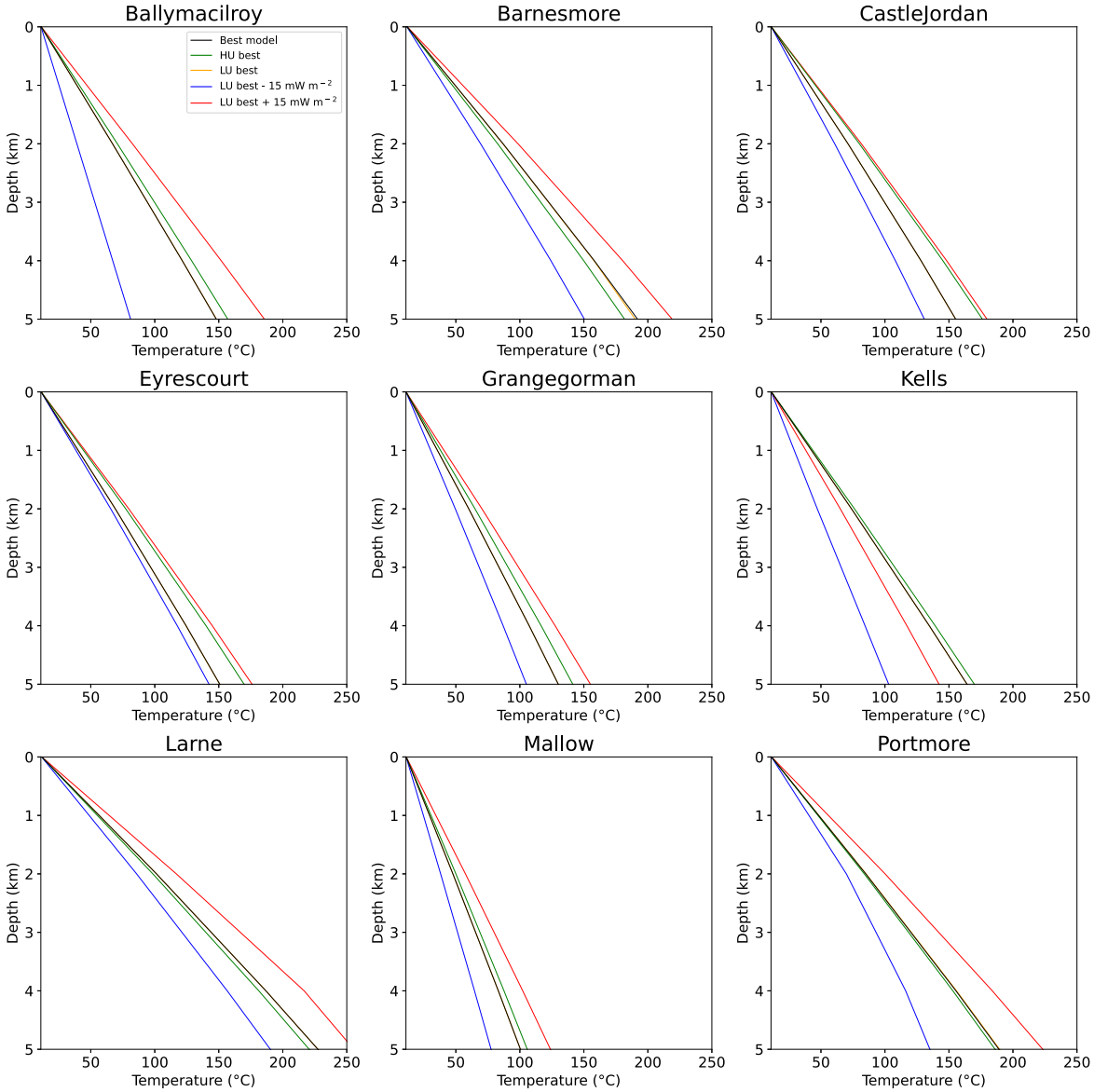

Figure 9. SHF sensitivity tests for each of the nine columns. The original best model is shown by the black line and the green line is the best model with uncertainty in the SHF data increased to 15 mW m^{-2} (HU = High uncertainty). The orange, blue and red lines are the second set of test for LU = Low Uncertainty, with orange the original SHF value, blue -15 mW m^{-2} from the original and red $+15$ mW m^{-2}. Uncertainty in the input data was reduced to 0.0001. As expected, the best and LU best models are very similar with the HU best model also close to the original best model.

5.3 3-D lateral heat flow modelling

The 1-D inversion assumes vertical conduction within a column and ignores lateral heat flow. To assess the potential effects of lateral heat flow we performed a 3-D thermal forward simulation using the integrated 3-D modelling software LitMod3D (Fullea *et al.* 2009). The 3-D input model was based exclusively on the output of the pseudo 3-D volume created from the collated 1-D inverted columns and was parametrized at a 10 km grid spacing. The inputs included boundaries for the crust, LAB and Moho depths, as well as the output crustal RHP and TC which were assigned to the three crustal layers.

The output 3-D forward models for both temperature and SHF (Supplementary Fig. 7) are similar to the 1-D fields in the different columns and contain the same large-scale patterns. The 1-D to 3-D differences in most of the model points are within $\pm$ 4 °C, however, the 3-D temperature field is smoother than the 1-D, particularly for small-scale structures. The largest variation is 16 °C at the Galway granite which is still observed as a warm spot in the 3-D model though not as significant as the 1-D. For the SHF the largest difference is $\pm$15 mW m^{-2} with most points within $\pm$6 mW m^{-2}. This is expected as the 1-D version has no information from neighbouring structures which would trade off with one another if the lateral contrasts in thermal properties were large. In areas with large lateral changes in topography, such as at the coast, the vertical discretization may also influence the output for the 3-D model, however we kept it at 2 km vertical discretization to match the 1-D version. The variations between the 1-D model and a 3-D forward model based on the 1-D, are larger than the uncertainties based on the setup of the 1-D inversion which we describe in the uncertainty analysis in Section 5.1.

5.4 Results of the uncertainty analysis

The uncertainty analysis suggests the temperature uncertainty is ∼3.5 °C at 2 km depth, presented in Fig. 6 and Fig. 8. These uncertainties are lower bound estimates given the limitations in our 1-D thermal modelling neglecting 3-D effects, and in the lateral averaging applied to the upper crustal lithology (see Section 5.3), though all comparisons to direct borehole measurements are within these lower bounds, providing confidence in the uncertainty values. The uncertainty analysis also indicates we have confidence in most areas of our model with low RMS values. Supplementary Figs. 8 and 9 show the misfit for one column when changing Moho depth and LAB depth, and how the RMS changes based on each fixed input parameter. In contrast, the choice of input RHP and TC have a larger impact on the temperature uncertainty in our models (average RMS at 2 km depth ± 3 and 5 °C, respectively), whereas Moho and LAB depth show the lowest contributions (average RMS at 2 km depth of ∼ ±1 °C) (Supplementary Fig. 8). This is perhaps unsurprising based on the model setup and our focus on depths suitable for future geothermal exploitation (∼ 2 km). At crustal depths the temperature is mainly controlled by the thermal property information (TC and RHP). The LAB depth will modify the depth of the 1300 °C isotherm but will have less impact at 2 km depth. We also included SHF to show the variation in the RMS if this was included as an inversion parameter rather than data. This produces the highest overall RMS values and we investigated the SHF through a series of sensitivity tests.

The tests for extreme SHF and very low uncertainty (i.e. forcing the inversion to match the input SHF value) produced significantly higher misfit values and modified the resulting geotherms significantly (Fig. 9 and Supplementary Fig. 6). The temperature at 2 km depth changed by ± 35 °C in the most extreme case (Kells) and ±15 °C in the most minor case, and the RHP changed by a maximum of 0.8 μWm^{-3}. These values are a lot higher than the variations we expect from our model and highlight the importance of using the best input data possible and providing a realistic uncertainty value for any input datum. For our modelling, using a high uncertainty for the input data allows the temperature model to converge to a similar result within the predicted uncertainty.

5.5 Limitations

One of the limitations of this study is that while modelling in 1-D is appropriate for surface wave dispersion curve modelling and local isostasy, we do not account for lateral thermal effects such as lateral heat flow or heat refraction at individual bodies (as modelled in Section 5.3). In areas containing granite, radiogenic heat production will be higher and radiate in all directions from the body. Similarly, heat refraction will take place at the boundaries between geological units with very different thermal conductivities. We assume 1-D vertical heat conduction in the crust so in areas with high radiogenic heat production it is likely we underestimate the extent of their influence by neglecting lateral heat flow. One way to address these 1-D limitations is modelling the temperature field in 3-D (see Section 5.3), however this is computationally expensive and we obtain similar structures in both models. Given the limitations of parametrizing our 1-D inversion as discussed, it is likely that the actual subsurface temperature lies somewhere between the 1-D and the 3-D temperature models. Therefore, the uncertainty presented for the parameters in the 1-D inversion is likely a lower bound. Future work should include full 3-D integrated thermal modelling using gravity data in addition to the data sets already presented in this work, although this will significantly increase computing time.

The input data sets used in the 1-D inversion also have significant uncertainty, and while we try and account for a possible plausible range for input values within the uncertainty analysis, these could be larger than what we account for in this study. For example, the bedrock is assumed to be suitable for the upper crustal layer of the model, however if the bedrock is thin, this is likely not representative for this layer even though layer thickness (in a three-layered crustal model) is an inversion parameter. Unfortunately, without drilling or extensive geophysical surveys across the island of Ireland, we do not know the 3-D lithological structure of the whole crust so averaging the bedrock layer is a way to parametrize the upper crust layer.

TC data are also inherently variable for certain lithologies, such as limestone, with measurements on samples from the same unit changing by ±3 $W\,(m\,K)^{-1}$ (Long *et al.* 2018). Studies often provide the average TC rather than the variation of TC along the sample or with multiple measurements, with these having significant variability (e.g. Popov *et al.* 2016). Providing ranges for TC in the uncertainty analysis for each lithological unit allows us to see the typical variations. However, if the lithology is incorrectly assigned in a model column or if in a certain location the TC assigned to a particular unit is a significant outlier, then our predicted near-surface temperatures will be incorrect as well.

TC will also vary with depth (pressure), rock type and temperature. However, Chambers *et al.* (2023) showed that if an appropriate average constant value is used, then the predicted geotherm is similar to the case where a temperature and pressure-dependent TC is considered. Another problem with TC is that the lithologies chosen to assign TC are sometimes too broad in previous studies. For example, in Table 1 row 1, a unique value for all volcanic rocks is used. This will result in an increased TC for basalts (which typically have low TC) whereas TC for granites will be underestimated due to averaging with other volcanic unit measurements.

RHP is also significantly averaged with certain rock units likely to be higher than others. As we average RHP for the whole crust in our models we cannot determine the depth extent of individual lithologies such as granites, rather we can say they are likely thicker/thinner or more/less radiogenic. Using a multilayered (i.e. upper, middle and lower crust) value for RHP will make a difference to our output temperature gradient in the crust. In Supplementary Fig. 10 we show tests for a 3-layer model using the same RHP value for all the layers (i.e. uniform RHP as in our inversion setting) and then two further tests where the average RHP is kept constant but the RHP in the upper crustal layer is increased or decreased by 0.2 $\mu W\,m^{-3}$ and the middle and lower crust are balanced to keep the same whole crustal average (Supplementary Table 1). Assuming a higher RHP in the upper crust and less in the middle and lower crust, the temperature increases almost negligibly (<1 K) in the upper crust but the temperature in the middle and lower crust significantly decreases (7–8 K). In contrast, if the RHP in the upper crust is decreased while the middle and lower RHP is increased keeping the average the same, we observe a reduction in temperature in the uppermost crust but an increase in temperature in the middle and lower crust (Supplementary Fig. 10). In future work, the crustal RHP should be varied per layer not as one crustal average.

Another source of uncertainty is in our comparison to borehole temperature. The time difference between the borehole drilling and the actual temperature measurement has an impact, and this information is not included for most boreholes in Ireland. Both the time taken to drill a borehole and the time since fluid circulation will impact so a simple value for time after drilling cannot be given,

but this can be many months after drilling for the borehole to equilibrate. This can cause variations in excess of 10 °C for bottom hole temperatures (Deming 1989). Similarly, the subsurface temperature will have been affected by surface effects in the upper few hundred metres and paleoclimate effects down to a few kms. Although paleoclimate effects can be as much as 6 °C at 2 km depth, for the majority of temperature measurements in Ireland this effect is only about 2 °C at 500 m, (Mather *et al.* 2018). Our model does not include paleoclimate effects as the input SHF data have already been corrected. Some of the direct temperature measurements have been corrected for paleoclimate effects, though not all provide information on this, therefore the differences between the model and borehole temperatures could be larger than what we estimate in this work. Additionally, the borehole temperature measurements do not provide information on fluids and we do not correct for convection in the borehole which can vary by ± 3 °C in the upper 50 m though decreases to ± 0.05 °C beyond 200 m (e.g. Eppelbaum & Kutasov 2011).

6 DISCUSSION

6.1 Temperature models, radiogenic heat production and geothermal applications

Temperatures in Ireland range from < 50 to 90 °C at 2 km depth (Fig. 2 and Supplementary Fig. 2). The warmest temperatures are located beneath areas with known granitic intrusions and areas of thinner crust such as the NE of Ireland. At 5 km depth the Galway and Donegal granitic regions exceed 180 °C similar to some of the highest temperatures observed in the UK which are being explored for future electricity generation (Abesser *et al.* 2020).

Most of the RHP values are within the typical ranges for bulk crustal RHP [0.74 to 1.38 μW m^{-3} (Vilà *et al.* 2010; Jaupart *et al.* 2016)]. The radiogenic heat production is closely tied to the input SHF with areas of high SHF having high RHP predicted in our models. However, there are some variations such as the Mourne granites which appear to have higher RHP than the SHF map. The RHP in the south of the island of Ireland is low for continental Phanerozoic terranes (<0.7 μW m^{-3}) and suggests that the low SHF value which comprises only a single data point is potentially inaccurate and additional temperature measurements should be taken. This low SHF and resulting RHP in the south will result in lower temperatures in the model, which in reality may be higher if more realistic crustal RHP values are considered. There are no deep boreholes in this region to compare the model to, but it is likely that the temperature could be higher than the models predict due to limited input data.

The granitic regions have high radiogenic heat production both in our output model (Fig. 5 average of whole crust) and in previous studies (Fig. 1f) which would result in elevated temperatures for the models. The RHP is variable for each granitic area, with high RHP beneath the Donegal granites and moderately elevated heat production for the Galway and Mourne granites. In contrast, the Leinster granites have RHP ∼1.2 μW m^{-3}, which is similar to the crustal averages for RHP (Jaupart *et al.* 2016). Similarly, the edges of the Galway granite have some of the lowest RHP in the model. TC is also low in our models for areas with granite, compared to global averages (Somerton 1992; Clauser & Huenges 1995; Cho *et al.* 2009; Long *et al.* 2018), due to the assigned TC being a combination of granite and other lithologies such as basaltic units which have a low TC (Table 1 Row 1–Volcanics). These would potentially be higher if TC had been split into a purely granitic unit which was not the case for Chambers *et al.* (2023) who had too few TC measurements on granites from previous studies to make a separate sub-group. Crustal and lithospheric thicknesses are also variable for the individual granitic regions suggesting the radiogenic heat production is the primary driver for the elevated temperatures in these areas.

The Leinster granites are cooler than the Galway and Donegal granites, suggesting a difference in the composition or thickness of these units. Due to our 3-layered crust we cannot constrain their thickness. The RHP for this granitic region is also the lowest for the model (Fig. 5). Previous studies reported a range of radiogenic heat production rates for the different Irish granites, with the lowest in Leinster (Willmot Noller & Daly 2015). This would result in cooler temperatures and a lower geothermal gradient, which matches well to the output RHP (Fig. 5) and is consistent with the temperature maps in our models (Fig. 2). The lateral extent of these bodies will be larger than this model as we take the surface extent of the bedrock geology to be the same for the whole upper crust, resulting in a minimum temperature estimate for the granite. The inversion is also performed on 1-D columns which assume no lateral heat flow, though the SHF partly corrects for this by being higher over granitic bodies. The limited measurements for SHF reduce its influence, however (Mather *et al.* 2018). The subsurface extent from seismic, gravity and electrical resistivity models provides evidence for larger lateral extent than observed in these models (O'Donnell *et al.* 2011; Yeomans 2011; O'Reilly *et al.* 2012; Delhaye *et al.* 2017, 2019) and therefore our temperature estimates for these areas are likely a lower bound.

The Mourne granites are similar to the Leinster granites and are not hotter than average in this model, unlike the other granitic regions. There are several potential reasons for this. First, the surface extent of the granite has been averaged with mudstone and sandstone layers when selecting a 20 km area, which affects the assigned TC. The SHF data are not elevated, in contrast to the Galway and Donegal granites, which would also result in lower temperatures in the model. Previous studies of Irish granites have found compositional differences between the granites of the Mourne Mountain Complex and the Galway, Donegal and Leinster granites and this is reflected in the measured SHF (Mather *et al.* 2018). The latter granites are more acidic and are visible as negative gravity anomalies, in contrast to the Mourne granites which have a positive gravity anomaly signature and have been associated with the presence of a denser mafic body located beneath the exposed granitic rocks (Reay 2004; Yeomans 2011). Given the high shallow RHP [some of the highest values in Ireland (Willmot Noller & Daly 2015)], it is likely that this area is warmer than our model suggests or is volumetrically small and shallow.

The Antrim Lava Group in Northern Ireland is located on top of some of the warmest temperatures of the model. Previous studies suggest this area has low surface heat flow (Mather *et al.* 2018) and the thermal conductivity of this unit is low, <2.0 W $(m\ K)^{-1}$ (Wheildon *et al.* 1985; Gebski *et al.* 1987; Raine & Reay 2019; Chambers *et al.* 2023). Similarly, the RHP is low to moderate in the model (Fig. 5). The basalt sequences range from 10′s to 100′s of metres thick (Delhaye *et al.* 2017, 2019; Raine & Reay 2019) and these overlie more thermally conductive and radiogenic limestone and sandstone units (Raine & Reay 2019; English *et al.* 2022, 2023). Therefore, the basalt units are likely acting as an insulating layer (cap rock), trapping heat rising from the mantle in a sandstone geothermal reservoir characterized by a thin and hot lithosphere.

The coolest areas in our model are in the Midlands and the southwest of the island (<52 °C at 2 km depth, Fig. 2). The Midlands

of Ireland were modified during the Caledonian orogeny which left a thickened lithosphere with respect to the surrounding Irish terranes as an imprint. As the LAB is deeper, the mantle heat source is farther from the surface resulting in cooler geotherms as observed in this work and Chambers *et al.* (2023). A potentially surprising cool region is Mallow, Co. Cork (Fig. 2, bottom right panel, indicated by an M). It is an area with thick lithosphere and there are extensive carbonate sequences which have a lower TC than the granites (Long *et al.* 2018; Chambers *et al.* 2023) and SHF & RHP measurements for the area are relatively low (Willmot Noller & Daly 2015; Mather *et al.* 2018) which agree with the temperature models that this is a relatively cool region. However, this area is known for its warm springs, which are in use to heat a swimming pool, suggesting the geothermal potential of an area is closely related to the ability to bring heat from depth up to the surface. Deep penetrating faults to allow fluid circulation are known in this area (Meere & Banks 1997). Therefore, our model suggests at 2 km depth, temperatures are everywhere sufficient for heating if the heat can be extracted to the surface [temperatures required for heating: 60 °C and electricity generation: >150 °C (DECC 2020, 2024)].

The modelled geothermal gradient ranges from < 20 to ∼40 °C km^{-1} in the upper crust (Fig. 3). In Northern Ireland where there are some of the highest gradients (>30 °C km^{-1}), formation fluids should be suitable for large-scale direct heating uses (Pasquali *et al.* 2010, 2015; Raine & Reay 2019). These gradients are close to those in Southampton, and for the United Downs and Eden Geothermal deep geothermal projects in southwestern GB (Beamish & Busby 2016; Farndale *et al.* 2022). The geothermal gradients we observe in Northern Ireland are significantly higher than the previously estimated averages for the area (Wheildon *et al.* 1985; Busby *et al.* 2011; Busby 2014; Beamish & Busby 2016; Raine & Reay 2019; Parkes *et al.* 2020; Farndale *et al.* 2022).

At 2 to 3 km depth temperatures would be sufficient for combined heat and power generation, with the Rathlin Basin, Larne Basin, Lough Neagh Basin, western Donegal and Galway granites being the best candidates for this combined deep geothermal use. Previous studies suggested the Rathlin Basin would have the highest geothermal gradient when compared to Lough Neagh and Larne basins. However, the original geothermal gradients were calculated on temperature data taken directly after drilling as bottom hole temperature measurements, when the temperatures were likely cooler due to circulating mud (Pasquali *et al.* 2010, 2015; Raine & Reay 2019). The geothermal gradient determined by our model of ∼35°C km^{-1} from the Ballinlea-1 well in the Rathlin Basin (English *et al.* 2022, 2023), is consistent with the previous studies suggesting the higher geothermal gradients at Lough Neagh (35°C km^{-1}) and Larne (38.5 °C km^{-1}) are likely correct and significantly higher than the 32 and 28 °C km^{-1} values previously suggested (Pasquali *et al.* 2010). In any case, areas with the lowest geothermal gradients could still be sufficient for heating purposes as evidenced in Mallow. Future studies should focus on the availability of fluids and fluid pathways that bring heat to the surface, and are already in progress as part of the DIG project.

6.2 LAB and moho depth

The new LAB depth derived in this study (Fig. 7b), ranges from 76 to 112 km deep. The new model suggests thicker lithosphere in southern, central and eastern Ireland which trends northwest–southeast. South of the Iapetus Suture Zone the LAB is deeper while to the north, the LAB is shallower. This thinning of the lithosphere from southwest to northeast may indicate the boundary between the Avalonian and Laurentian domains when the two supercontinents collided during the Caledonian orogeny. This is consistent with previous studies of seismic data and geological evidence (Chew & Stillman 2009; A. G. Jones *et al.* 2014; Fullea *et al.* 2014; Bonadio *et al.* 2021). In contrast, Landes *et al.* (2007) did not find a thicker lithosphere beneath the Iapetus Suture Zone, though this may be due to a sparse input data set producing smooth models capturing only the first order south to north lithospheric thinning trend.

Previous estimates of LAB depth are variable, with depths of 55 to 85 km for a S-to-P receiver function study (Landes *et al.* 2007), 85 to 145 km thick from a joint modelling of gravity, magnetic and elevation data with a seismically derived Moho depth (Baykiev *et al.* 2018) and 95 to 105 km when the Moho was constrained by gravity rather than seismic data in the same study. 1-D surface wave models for Ireland suggest the LAB ranges from 60 to 100 km depth in Ireland (Bonadio *et al.* 2021; Lebedev *et al.* 2024). The work of Landes *et al.* (2007) suggested the LAB was anomalously shallow everywhere in Ireland, either from thinning by thermal erosion from the proto-Icelandic plume head or from Ireland being the transition from oceanic to continental crust, though this boundary is expected far offshore to the west of Ireland. A joint inversion using gravity, elevation and mantle compositions produced an LAB map ranging from 85 km thick in the north increasing to 115 km in the south, consistent with the model shown here. The Landes *et al.* (2007) model required a minimum lithospheric thickness of 85 km, otherwise topographic variations could not be reconciled (Jones *et al.* 2014). The model shown here has more detail and is less smooth than previous studies, which is due to the larger volume of input seismic data used in the inversions allowing us to more accurately map the lithospheric boundary.

The thinnest lithosphere, of the model, is in the north of the island of Ireland where the Antrim Lava Sequence is located and in the east beneath Belfast and the Strangford Lough region. The extensive volcanic sequences in the area suggest the lithosphere could have been thinned during their emplacement which previous studies have suggested was from thermal erosion in the past from the Icelandic plume (Landes *et al.* 2007; Bonadio *et al.* 2021).

The new Moho map ranges from 25 to 33 km depth (Fig. 7a) and shows similar trends to the LAB map. The Moho map is similar to previous seismic and joint inversion models with greater detail and some differences (A. G. Jones *et al.* 2014; Fullea *et al.* 2014; Baykiev *et al.* 2018; Bonadio *et al.* 2021; Licciardi *et al.* 2014, 2020).

The thinnest crust is in the north and west of the island of Ireland. In Northern Ireland the thin crust coincides with an area with known warm temperatures from the Portmore (Fig. 4) and Ballinlea-1 boreholes (Chambers *et al.* 2023). The elevated temperature in these boreholes reflects both the lithology (porous quartz rich sandstone with a high TC, capped with a low TC basalt) and this study suggests these temperatures are also high due to the thin lithosphere. In addition, given the thin Moho occurs beneath the Antrim Lava Sequence, the shallower Moho depths likely reflect thinning induced by the Icelandic plume (Bonadio *et al.* 2021) and/or crustal extension of the Larne and Rathlin basins (Landes *et al.* 2005; O'Reilly *et al.* 2010). A shallower Moho is also observed towards the west in Connemara and Mayo which is visible on the input Moho map (Fig. 1). Given limited evidence for basin extension or volcanic intrusive centres in this area, it is possible the thinner crust present in the input data is influencing the output.

The deepest Moho is observed in central and southern Ireland following the broad trend of the Iapetus Suture Zone. We attribute

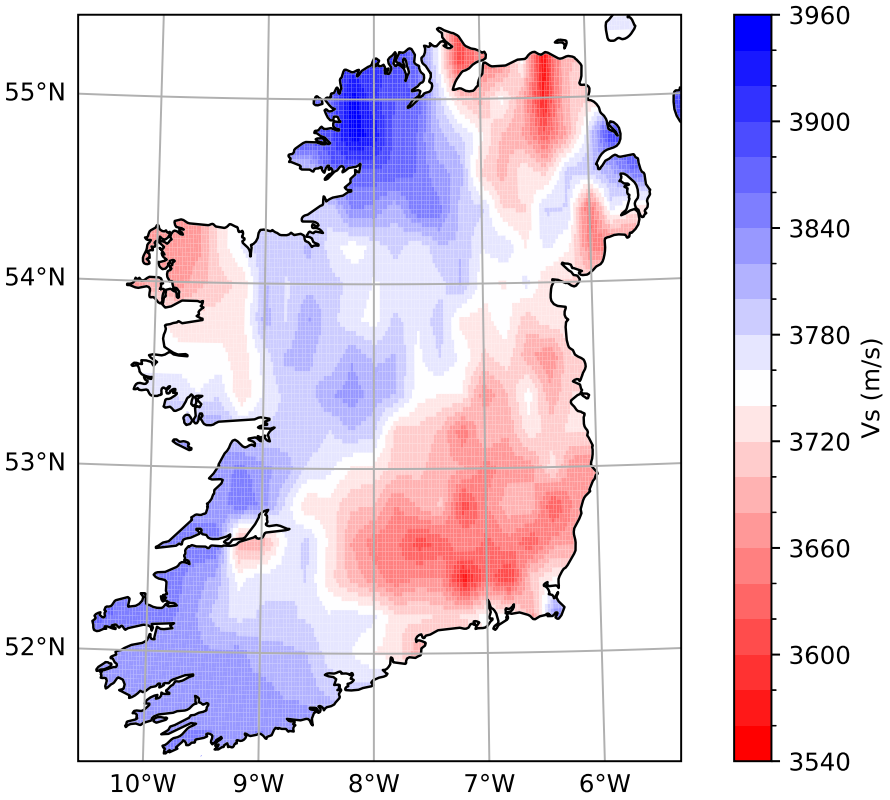

Figure 10. Average shear wave velocity (Vs) of the middle and lower crust weighted by layer thickness derived from our 1-D inversions.

this thickened crust to compression during the collision of the Avalonian and Laurentian terranes. Moho depths from Ireland derived from gravity data and isostatic modelling suggest the Moho is 27 to 30.5 km deep (Baykiev *et al.* 2018) showing a smoothed pattern at odds with our results. However, when crustal seismic data (controlled source and receiver functions) was included the jointly inverted Moho ranges from 27 to 34 km, which is more similar to our model results (25 to 33 km).The new state-of-the-art LAB and Moho depth maps provide fundamental information for future studies investigating the tectonic evolution of the island of Ireland and its geothermal and mineral resources.

Another output from the inversion is shear wave velocity (Vs) for each crustal layer. The input surface waves are less sensitive to the upper crust due to limited short period information so we use an average of the middle and lower crust only. As the layer thicknesses vary, we plot an average crustal velocity weighted according to the thickness of each layer (Fig. 10). In general, we observe lower Vs in the southeast and beneath the Antrim lava sequence, with higher Vs in the northwest and western most Ireland. Particularly notable are areas of high Vs corresponding with high RHP and SHF regions and vice versa. There is less similarity between Vs and the Moho and LAB depths. In the Mourne granites, we observe low to moderate Vs. Gravity studies and previous models have required high density values in the crust for this region, which may suggest that igneous intrusions, occasionally exposed, for example, in roadcuts around Newry, are also present in the subsurface (Fullea *et al.* 2014).

To improve the temperature models in the future, this methodology could be adapted for regional refinement using more advanced crustal thermal property data at a finer grid spacing. For example, TC changes with lithology and could be varied at a finer resolution than the seismic data sets which are constrained to their own resolution. This would allow better matches to measured geothermal gradients in regions where there are rapid changes in lithology. In addition, better knowledge of the subsurface, including the depth extent of lithological units could be gained by utilizing new gravity and MT data sets being gathered and processed in Ireland (Kiyan *et al.* 2023). This would improve assignment of thermal properties and crustal geometries and hence improve the robustness of the temperature model. In addition, new and well-constrained heat flow data are also necessary. These data sets should then be combined with a multilayer crustal inversion, including sediment layers and additional gravity data constraints in a 3-D framework (in contrast to the 1-D version used here to produce a pseudo 3-D model), able to account for lateral heat flow. Obtaining Vp information for a 3-D model would also be useful to obtain more detailed information on the crustal structure, which, in turn, will support more accurate temperature models. Finally, the thermal conductivity ranges were based on an averaged model for each rock type based on limited Irish rock measurements. More TC measurements should be taken, and the full range of values tested rather than an average for each lithological unit. Finally, more deep temperature measurements in deep boreholes are required to ground truth and improve the models.

7 CONCLUSIONS

In this paper new subsurface temperature (Fig. 2) maps with uncertainty have been computed for Ireland based on joint geophysical–petrological inversion of surface wave, SHF and petrophysical data sets. The models have also been compared to direct borehole temperature measurements where available, with modelled temperatures showing good agreement with the observations. The addition of uncertainty to the final temperature models provides a reliable

resource that can be used for risk analysis in developing future projects and further exploration as uncertainty allows a definition of risk. The temperature and geothermal gradient maps (Fig. 3) indicate a higher geothermal gradient for Ireland than previously reported, suggesting temperatures everywhere at 2 km depth are sufficient for residential and industrial heating purposes. The warmest areas in Ireland according to our models coincide with granites and the Antrim Lava Sequence. The hottest granite areas are in counties Donegal and Galway likely reflecting higher amounts of radiogenic elements in these rocks compared, for example, to the Leinster granites.

New high-resolution LAB and Moho depth (Fig. 7) maps have been produced with the most up-to-date geophysical data and are the current state-of-the-art with more detail than previous models. The coolest areas in the Iapetus Suture Zone and south of Ireland are also the areas with the thickest crust and lithosphere in our models. This thickening in the Iapetus Suture Zone is likely the result of the collision between Avalonia and Laurentia. Areas with thinner lithosphere typically have warmer temperatures. The Moho depth map also has areas of thinned crust in the north of the island of Ireland, particularly beneath the Antrim Lava sequence and the Larne and Rathlin basins, suggesting extension has thinned the crust along with thermal erosion from a past mantle plume.

New maps of crustal RHP (Fig. 5) correlate well to the temperature maps suggesting, in general, areas with thicker crust have higher RHP, which may reflect more felsic crustal compositions in the midlands. Similarly, the RHP map shows variations within the granitic areas suggesting areas with higher SHF and consequently RHP are likely to have warmer temperatures such as in Co. Donegal and Galway.

This work shows how parametrizing the crust in great detail allows us to scale the workflow for a whole region. This was possible by having large data sets used as input parameters/variables which were available as grids for the region. The uncertainty analysis is specifically tailored to shallow temperature estimates making it useful for the geothermal community and allows assessment of risk for the final temperature models. Future studies could utilize the workflow for areas with similar sparse data sets enabling a better understanding of the geothermal potential and determining areas suitable for further exploration and exploitation. This will be essential in the near future for energy self-sufficiency, meeting green energy targets and moving to green energy sources.

ACKNOWLEDGMENTS

We thank GSI and GSNI for providing access to geological maps, thermal conductivity data and for fruitful discussions. The DIG project is funded by the Sustainable Energy Authority of Ireland and Geological Survey Ireland under the Sustainable Energy Authority of Ireland Research, Development & Demonstration Funding Programme 2019 (grant number 19/RDD/522). ELC is funded under the Science Foundation Ireland - Irish Research Council (now Research Ireland) Pathway Programme 22/PATHS/10676 and the Sustainable Energy Authority of Ireland Research and Development & Demonstration Funding Programme 2022, Grant number 2022/RDD/782. JF is supported by projects PID2020-114854GB-C22 and CNS2022-135621 funded by the Spanish Ministry of Science and Innovation. Additional support from Project InnerSpace (https://projectinnerspace.org) and project 4D Dynamic Earth, funded by European Space Agency (4000140327/23/NL/SD) as part of EXPRO+, is gratefully acknowledged. We gratefully acknowledge the support of the iCRAG Centre, which is funded by Science Foundation Ireland (now Research Ireland) grants 13/RC/2092 and 13/RC/2092_P2 and cofunded under the European Regional Development Fund. Heat Production Rate data were acquired during the IRETHERM project, which was funded by Science Foundation Ireland (now Research Ireland) (grant number 10/IN.1/I3022). Additional support from the UK Natural Environment Research Council Grant Number NE/X000060/1 and the Science Foundation Ireland (now Research Ireland) Grant Number 16/IA/4598, cofunded by Geological Survey Ireland and the Marine Institute, is acknowledged.

We thank Dr Henri Samuel and three anonymous reviewers for their feedback and comments on the manuscript.

SUPPORTING INFORMATION

Supplementary data are available at *GJIRAS* online.

Please note: Oxford University Press is not responsible for the content or functionality of any supporting materials supplied by the authors. Any queries (other than missing material) should be directed to the corresponding author for the paper.

DATA AVAILABILITY

The final Temperature model with uncertainty, LAB and Moho maps are available through Geological Survey Ireland's map viewer (https://experience.arcgis.com/experience/46ef92b5b58d41bc98e0d97e7a779cf2, www.gsi.ie/en-ie/data-and-maps/Pages/default.aspx) and on the DIAS Access to Institutional Repository (DAIR) (https://dair.dias.ie/id/eprint/1410/& https://dair.dias.ie/id/eprint/1424).

REFERENCES

Abesser, C., Busby, J.P., Pharaoh, T.C., Bloodworth, A.J. & Ward, R.S. 2020. *Unlocking the potential of geothermal energy in the UK Decarbonisation and Resource Management Programme, Open Report OR/20/049,* British Geological Survey.

Afonso, J., Fullea, J., Griffin, W., Yang, Y., Jones, A., D Connolly, J. & O'Reilly, S., 2013. 3-D multiobservable probabilistic inversion for the compositional and thermal structure of the lithosphere and upper mantle. I: a priori petrological information and geophysical observables, *J. geophys. Res.,* **118,** 2586–2617.

Afonso, J.C., Fernàndez, M., Ranalli, G., Griffin, W.L. & Connolly, J.A.D. 2008. Integrated geophysical-petrological modeling of the lithosphere and sublithospheric upper mantle: methodology and applications, *Geochem. Geophys. Geosyst.,* **9**(5).

Amante, C. & Eakins, B.W. 2009. ETOPO1 1 Arc-Minute Global Relief Model: procedures, Data Sources and Analysis, *NOAA Technical Memorandum NESDIS NGDC-24. National Geophysical Data Center, NOAA,*

Anikiev, D., Lechel, A., Laura Gomez Dacal, M., Bott, J., Cacace, M. & Scheck-Wenderoth, M. 2019. A three-dimensional lithospheric-scale thermal model of Germany, *Adv. Geosci.,* **49,** 225–234.

Artemieva, I.M. & Mooney, W.D. 2001. Thermal thickness and evolution of Precambrian lithosphere: a global study, *J. geophys. Res.: Solid Earth,* **106**(B8), 16387–16414.

Axelsson, G., Gunnlaugsson, E., Jónasson, T. & Ólafsson, M. 2010. Low-temperature geothermal utilization in Iceland—Decades of experience, *Geothermics,* **39**(4), 329–338.

Baptie, B.J. 2018. Earthquake Seismology 2017/2018, *British Geological Survey,* **OR/18/029,** 1–42. http://earthquakes.bgs.ac.uk/publications/annual_reports/2018_29th_annual_report.pdf

Bartzsch, S., Lebedev, S. & Meier, T. 2011. Resolving the lithosphere-asthenosphere boundary with seismic Rayleigh waves, *Geophys. J. Int.,* **186**(3), 1152–1164.

Baykiev, E., Guerri, M. & Fullea, J. 2018. Integrating gravity and surface elevation with magnetic data: mapping the curie temperature beneath the British Isles and surrounding areas, *Front. Earth Sci.,* **6**(October), 1–19.

Beamish, D. & Busby, J. 2016. The Cornubian geothermal province: heat production and flow in SW England: estimates from boreholes and airborne gamma-ray measurements, *Geotherm. Energy,* **4**(1).

Békési, E. *et al.* 2018. Subsurface temperature model of the Hungarian part of the Pannonian Basin, *Global Planet. Change,* **171,** 48–64.

Békési, E. *et al.* 2020. An updated geothermal model of the Dutch subsurface based on inversion of temperature data, *Geothermics,* **88,** 101880.

Blacknest 1960. *UK-Net, Blacknest Array [Data set],* International Federation of Digital Seismograph Networks.

Blake, S. *et al.* 2016a. Understanding hydrothermal circulation patterns at a low-enthalpy thermal spring using audio-magnetotelluric data: a case study from Ireland, *J. Appl. Geophys.,* **132,** 1–16.

Blake, S. *et al.* 2021. Characterising thermal water circulation in fractured bedrock using a multidisciplinary approach : a case study of St. Gorman ' s Well, Ireland, *Hydrogeol. J.,* **29**.

Blake, S., Henry, T., Murray, J., Flood, R., Muller, M.R., Jones, A.G. & Rath, V. 2016b. Compositional multivariate statistical analysis of thermal groundwater provenance: a hydrogeochemical case study from Ireland, *Appl. Geochem.,* **75,** 171–188.

Blake, T., Lebedev, S., O'Reilly, B.M., Agostinetti, N., Agius, M.R. & Schaeffer, A.J. 2012. An unusual occurrence of a moderately sized earthquake (Ml 4.2) on the Irish continental shelf and passive margin, *AGU Fall Meeting Abstracts, 2012,* S53A–2476.

Bonadio, R. *et al.* 2021. Optimal resolution tomography with error tracking and the structure of the crust and upper mantle beneath Ireland and Britain, *Geophys. J. Int.,* **226**(3), 2158–2188.

Brock, A. 1989. Heat flow measurements in Ireland, *Tectonophysics,* **164**(2–4), 231–236.

Brock, A. & Barton, K.J. 1984. Equilibrium Temperature and Heat Flow Measurements in Ireland, **Contract no. EG-A-1-022-EIR(H),** 1–144.

Busby, J. 2014. Geothermal energy in sedimentary basins in the UK, *Hydrol. J.,* **22**(1), 129–141.

Busby, J., Kingdon, A. & Williams, J. 2011. The measured shallow temperature field in Britain, *Q. J. Eng. Geol. Hydrogeol.,* **44**(3), 373–387.

Cammarano, F., Goes, S., Vacher, P. & Giardini, D. 2003. Inferring upper-mantle temperatures from seismic velocities, *Phys. Earth planet. Inter.,* **138**(3–4), 197–222.

Campanyà, J., Jones, A.G., Vozár, J., Rath, V., Blake, S., Delhaye, R. & Farrell, T. 2015. Porosity and Permeability Constraints from Electrical Resistivity Models: examples Using Magnetotelluric Data, *Proceedings World Geothermal Congress 2015,* Melbourne, Australia 19-25 April 2015, www.iretherm.ie

Chambers, E.L. *et al.* 2023. Determining subsurface temperature and lithospheric structure form joint geophysical-petrological inversion: a case study from Ireland, *Tectonophysics,* **869,** 230094.

Chew, D.M. & Stillman, C.J. 2009. Late Caledonian orogeny and magmatism, in *The Geology of Ireland,* pp. 143–173, Holland, C. H. & Sanders, I. S., Dunedin Academic Press.

Cho, W.J., Kwon, S. & Choi, J.W. 2009. The thermal conductivity for granite with various water contents, *Eng. Geol.,* **107**(3–4), 167–171.

Clauser, C. & Huenges, E. 1995. Thermal conductivity of rocks and minerals, in *Rock Physics and Phase Relations: A Handbook of Physical Constants,* vol. **3,** pp. 105–126, ed. Ahrens, T. J., American Geophysical Union.

Cloetingh, S.A.P.L. *et al.* 2010. Lithosphere tectonics and thermo-mechanical properties: an integrated modelling approach for Enhanced Geothermal Systems exploration in Europe, *Earth Sci. Rev.,* **102,** 3–4, 159–206.

Connolly, J. & Kerrick, D., 2002. Metamorphic controls on seismic velocity of subducted oceanic crust at 100–250 km depth, *Earth planet. Sci. Lett.,* **204,** 61–74.

Connolly, J.A.D. 2005. Computation of phase equilibria by linear programming: a tool for geodynamic modeling and its application to subduction zone decarbonation, *Earth planet. Sci. Lett.,* **236**(1–2), 524–541.

Cooper, M.R. 2004. Antrim Lava Group, Palaeogene extrusive igneous rocks, Northern Ireland, in *The geology of Northern Ireland-our natural foundation. Geological Survey of Northern Ireland, Belfast,* ed. Mitchell, W. I., British Geological Survey. https://earthwise.bgs.ac.uk/index.php/Post-Variscan_deformation_and_basin_formation,_Northern_Ireland

Cooper, M.R., Anderson, H., Walsh, J.J., van Dam, C.L., Young, M.E., Earls, G. & Walker, A. 2012. Palaeogene alpine tectonics and icelandic plume-related magmatism and deformation in Northern Ireland, *J. Geol. Soc.,* **169**(1), 29–36.

Cooper, M.R., Crowley, Q.G. & Rushton, A.W.A. 2008. New age constraints for the Ordovician Tyrone Volcanic Group, Northern Ireland, *J. Geol. Soc.,* **165,** 333–339. https://www.lyellcollection.org

Daly, J.S. 2009. Precambrian, in *The Geology of Ireland,* pp. 7–42, eds Holland, C. H. & Sanders, I. S., Dunedin Academic Press.

DECC, D. of T. E. C. and C. 2020. *Geothermal Energy in Ireland. A roadmap for a policy and regulatory framework,* Government of Ireland, 1–12, www.decc.gov.ie.

DECC, D. of T. E. C. and C. 2024. *Climate Action Plan 2024*. Government of Ireland, 1–420.

Delhaye, R., Rath, V., Jones, A.G., Muller, M.R. & Reay, D. 2017. Correcting for static shift of magnetotelluric data with airborne electromagnetic measurements: a case study from Rathlin Basin, Northern Ireland, *Solid Earth,* **8**(3), 637–660.

Delhaye, R., Rath, V., Jones, A.G., Muller, M.R. & Reay, D. 2019. Quantitative geothermal interpretation of electrical resistivity models of the Rathlin Basin, Northern Ireland, *Geothermics,* **77,** 175–187.

Deming, D. 1989. Application of bottom-hole temperature corrections in geothermal studies, *Geothermics,* **18**(5–6), 775–786.

Dewey, J.F. & Strachan, R.A. 2002. Caledonides of Britain and Ireland, *EUROPE/Caledonides of Britain and Ireland,* **2000,** 269–276.

DfE. 2021. *Policy Statement for Geothermal Energy for a Circular Economy Natura Impact Statement Natura Impact Statement*. Report, RPS Group, Natura Impact Statement, IE00095

Do, V.C., Readman, P.W., O'Reilly, B.M. & Landes, M. 2006. Shear-wave splitting observations across southwest Ireland, *Geophys. Res. Lett.,* **33**(3), 2–5.

Downing, R.A. & Gray, D.A. 1985. *Geothermal Energy: The potential in the United Kingdom,* Report, British Geological Survey, NERC, ISBN 0 11 884366 4

Downing, R.A. & Gray, D.A. 1986. Geothermal resources of the United Kingdom, *J. Geol. Soc.,* **143**(3), 499–507.

English, J.M., English, K.L., Dunphy, R.B., Blake, S., Walsh, J., Raine, R., Vafeas, N.A. & Salgado, P.R. 2023. An overview of deep geothermal energy and its potential on the island of Ireland, *First Break,* **41**(2), 33–43.

English, K., English, J.M., Dunphy, R., Blake, S., Walsh, J., Raine, R., Vafeas, N.A. & Rodriguez-Salgado, P. 2022. Deep Geothermal Potential on the Island of Ireland, in *3rd EAGE Global Energy Transition Conference & Exhibition,* pp. 1–5. European Association of Geoscientists & Engineers

Eppelbaum, L.V. & Kutasov, I.M. 2011. Estimation of the effect of thermal convection and casing on the temperature regime of boreholes: a review, *J. geophys. Eng.,* **8,** 1, R1–R10.

European Council. 2014. *2030 Climate and Energy Policy Framework,* EUCO 169/14, C) EUR 13, CONCL 5, Brussels.

Farndale, H., Law, R. & Beyon, S. 2022. An Update on the United Downs Geothermal Power Project, Cornwall, UK, *Conference Proceedings, 47th Workshop on Geothermal Reservoir Engineering Stanford University, Stanford, California,* Workshop on Geothermal Reservoir Engineering.

Farrell, T., Rath, V., Feely, M., Muller, M., Jones, A.G. & Brock, A. 2015. IRETHERM: the Geothermal Energy Potential of Radiothermal Granites in a Low-Enthalpy Setting in Ireland from Magnetotelluric Data, *Proceedings World Geothermal Congress 2015,* Melbourne, Australia, 19-25 April 2015.

Fellgett, M. & Monaghan, A.A. 2024. *User Guide: BGS UK Geothermal Catalogue first digital release, Legacy Data*. British Geological Survey

Förster, A., Fuchs, S., Förster, H.J. & Norden, B. 2021. Ambiguity of crustal geotherms: a thermal-conductivity perspective, *Geothermics,* 101937, **89**.

Frey, M., Bär, K., Stober, I., Reinecker, J., van der Vaart, J. & Sass, I. 2022. Assessment of deep geothermal research and development in the Upper Rhine Graben, *Geotherm. Energy,* **10**(1).

Freymark, J., Sippel, J., Scheck-Wenderoth, M., Bär, K., Stiller, M., Fritsche, J.G. & Kracht, M. 2017. The deep thermal field of the Upper Rhine Graben, *Tectonophysics,* **694,** 114–129.

Fridleifsson, G.O. & Elders, W.A. 2005. The Iceland Deep Drilling Project: a search for deep unconventional geothermal resources, *Geothermics,* **34**(3), 269–285.

Fritschle, T., Daly, J.S., Whitehouse, M.J., Buhre, S., Mcconnell, B. & Team, I. 2015. Geothermal Potential of Caledonian Granites Astride the Iapetus Suture Zone in Ireland and the Isle of Man-Implications for EGS Prospectivity, In *Proceedings World Geothermal Congress 2015,* Melbourne, Australia, 19-25 April 2015, www.iretherm.ie

Fullea, J., Afonso, J.C., Connolly, J.A.D., Fernàndez, M., García-Castellanos, D. & Zeyen, H. 2009. LitMod3D: an interactive 3-D software to model the thermal, compositional, density, seismological, and rheological structure of the lithosphere and sublithospheric upper mantle, *Geochem. Geophys. Geosyst.,* **10**(8), 1–21.

Fullea, J., Lebedev, S., Martinec, Z. & Celli, N.L. 2021. WINTERC-G: mapping the upper mantle thermochemical heterogeneity from coupled geophysical-petrological inversion of seismic waveforms, heat flow, surface elevation and gravity satellite data, *Geophys. J. Int.,* **226,** 146–191.

Fullea, J., Muller, M.R., Jones, A.G. & Afonso, J.C. 2014. The lithosphere-asthenosphere system beneath Ireland from integrated geophysical-petrological modeling II: 3D thermal and compositional structure, *Lithos,* **189,** 49–64.

Gan, Q., Feng, Z., Zhou, L., Li, H., Liu, J. & Elsworth, D. 2021. Down-dip circulation at the united downs deep geothermal power project maximizes heat recovery and minimizes seismicity, *Geothermics,* **96,** 102204.

Gebski, J.S., Wheildon, J. & Thomas-Betts, A. 1987. *Investigations of the UK heat flow field (1984-1987)*. Report, British Geological Survey, WJ/GE/87/6

Geological Survey Ireland. Geological Survey, Ireland, 2020. *Bedrock Geology Data and Maps*. Geological Survey Ireland, https://www.gsi.ie/en-ie/data-and-maps/Pages/Bedrock.aspx

Goodman, R., Jones, G.L., Kelly, J., Slowey, E. & O'Neill, N. 2004. *Geothermal Resource Map of Ireland. Final Report to Sustainable Energy Ireland*. Final report to Sustainable Energy Ireland. CSA rept no. 3085/02.04 September 2005. 93pp + XII App, CSA Group.

Graham, J.R. 2009. Ordovician of the North, in *The Geology of Ireland,* pp. 43–67, eds Holland, C. H. & Sanders, I. S., Dunedin Academic Press.

Hauser, F., O'Reilly, B.M., Readman, P.W., Daly, J.S. & van den Berg, R. 2008. Constraints on crustal structure and composition within a continental suture zone in the Irish Caledonides from shear wave wide-angle reflection data and lower crustal xenoliths, *Geophys. J. Int.,* **175**(3), 1254–1272.

Herrington, R.J., Hollis, S.P., Cooper, M.R., Stobbs, I., Tapster, S., Rushton, A., McConnell, B. & Jeffries, T. 2018. Age and geochemistry of the Charlestown Group, Ireland: implications for the Grampian orogeny, its mineral potential and the Ordovician timescale, *Lithos,* **302-303,** 1–19.

INSN. 1993. *Irish National Seismic Network (INSN) Operated by the Dublin Institute for Advanced Studies and Supported by the Geological Survey Ireland. International Federation of Digital seismograph networks*..

Jaupart, C., Mareschal, J.C. & Iarotsky, L. 2016. Radiogenic heat production in the continental crust, in *Lithos*vol. **262,** pp. 398–427, Elsevier B.V.

Johnston, T.P. 2004. Post-Variscan deformation and basin formation, Northern Ireland, in Mitchell, W. I., ed. *The geology of Northern Ireland-Our Natural Foundation. Geological Survey of Northern Ireland, Belfast,* DGeoplogical Survey of Northern Ireland, Cambridge University Press.

Jones, A.G., Afonso, J.C., Fullea, J. & Salajegheh, F. 2014. The lithosphere-asthenosphere system beneath Ireland from integrated geophysical-petrological modeling—I: observations, 1D and 2D hypothesis testing and modeling, *Lithos,* **189,** 28–48.

Jones, G.L., Goodman, R., Pasquali, R., Kelly, J.G., Neill, N.O. & Slowey, E. 2007. The Status of Geothermal Resource Development in Ireland, in *Proceedings European Geothermal Congress 2007* , Unterhaching, Germany, 30 May-1 June 2007.

Kassa, M., Alemu, A. & Muluneh, A. 2022. Determination of Conrad and Curie point depth relationship with the variations in lithospheric structure, geothermal gradient and heat flow beneath the central main Ethiopian rift, *Heliyon,* **8**(11), e11735.

Kennett, B.L., Engdahl, E.R. & Buland, R., 1995. Constraints on seismic velocities in the Earth from traveltimes, *Geophys. J. Int.,* **122**(1), 108–124.

Kiyan, D. *et al.* 2022. *Geothermal Study of Southern Ireland: DIG Project*. EGU General Assembly. EGU22–10526

Kiyan, D. *et al.* 2023. *3-D Magnetotelluric Assessment of the Georesources Potential of the Irish Crust*. EGU General Assembly. EGU23–16297

Landes, M., Ritter, J.R.R., Do, V.C., Readman, P.W. & O'Reilly, B.M. 2004. Passive teleseismic experiment explores the deep subsurface of southern ireland, *EOS, Trans. Am. geophys. Un.,* **85**(36), 337–341.

Landes, M., Ritter, J.R.R. & Readman, P.W. 2007. Proto-Iceland plume caused thinning of Irish lithosphere, *Earth planet. Sci. Lett.,* **255**(1–2), 32–40.

Landes, M., Ritter, J.R.R., Readman, P.W. & O'Reilly, B.M. 2005. A review of the Irish crustal structure and signatures from the Caledonian and Variscan Orogenies, *Terra Nova,* **17,** 2, 111–120.

Lebedev, S. *et al.* 2012. Ireland Array: a new broadband seismic network targets the structure, evolution and seismicity of Ireland and surroundings, in *EGU General Assembly Conference Abstracts,* Vienna, p. 3615.

Lebedev, S., 2022. The Ireland Array Working Group: Ireland Array, *GFZ Data Services,* Dataset/Seismic Network.

Lebedev, S., Adam, J.M.C. & Meier, T. 2013. Mapping the Moho with seismic surface waves: a review, resolution analysis, and recommended inversion strategies, *Tectonophysics,* **609,** 377–394.

Lebedev, S., Fullea, J., Xu, Y. & Bonadio, R. 2024. Seismic thermography, *Bull. seism. Soc. Am.,***114,** 1227–1242

Lebedev, S., Nolet, G., Meier, T. & Van der Hilst, R.D. 2005. Automated multimode inversion of surface and S waveforms, *Geophys. J. Int.,* **162**(3), 951–964.

Ledésert, B.A. & Hébert, R.L. 2020. How can deep geothermal projects provide information on the temperature distribution in the upper Rhine Graben? (The example of the soultz-sous-forêts-enhanced geothermal system), *Geosciences (Switzerland),* **10**(11), 1–24.

Lee, M.K., Brown, G.C., Webb, P.C., Wheildon, J. & Rollin, K.E. 1987. Heat flow, heat production and thermo-tectonic setting in mainland UK, *J. Geol. Soc.,* **144**(1), 35–42.

Lenkey, L. *et al.* 2017. Lithospheric scale 3D thermal model of the Alpine–Pannonian transition zone, *Acta Geod. Geophys.,* **52**(2), 161–182.

Licciardi, A., Agostinetti, N.P., Lebedev, S., Schaeffer, A.J., Readman, P.W. & Horan, C. 2014. Moho depth and Vp/Vs in Ireland from teleseismic receiver functions analysis, *Geophys. J. Int.,* **199**(1), 561–579.

Licciardi, A., England, R.W., Piana Agostinetti, N. & Gallagher, K. 2020. Moho depth of the British Isles: a probabilistic perspective, *Geophys. J. Int.,* **221**(2), 1384–1401.

Limberger, J. *et al.* 2018a. Geothermal energy in deep aquifers: a global assessment of the resource base for direct heat utilization, *Renew. Sustain. Energy Rev.,* **82**(October 2017), 961–975.

Limberger, J. *et al.* 2018b. Refining the thermal structure of the European lithosphere by inversion of subsurface temperature data, *Global Planet. Change,* **171,** 18–47.

Long, M., Murray, S. & Pasquali, R. 2018. Thermal conductivity of Irish rocks, *Irish J. Earth Sci.,* **36,** 63–80.

Maggio, G., Kiyan, D., Bean, C.J., Queralt, P., Delhaye, R., Hogg, C., Mcateer, J. & Blake, S. 2021. The GEO-URBAN Project: Exploring the Geothermal Potential of Dublin City using Electromagnetic and

Passive Seismic Methods, *Proceedings World Geothermal Congress 2020+1,* Reykjavik, Iceland, April - October 2021.

Maggio, G., Subašić, S. & Bean, C.J. 2022. Subsurface characterization using passive seismic in the urban area of Dublin City, Ireland, *Geophys. Prospect.,* **70**(8), 1432–1454.

Majorowicz, J., Polkowski, M. & Grad, M. 2019. Thermal properties of the crust and the lithosphere–asthenosphere boundary in the area of Poland from the heat flow variability and seismic data, *Int. J. Earth Sci.,* **108**(2), 649–672.

Masters, G., Barmine, M. & Kientz, S. 2007. *Mineos User'S Manual. Computational Infrastructure for Geodynamics*. California Institute of Technology, Pasadena, http://geodynamics.org/cig/software/mineos.

Mather, B., Farrell, T. & Fullea, J. 2018. Probabilistic surface heat flow estimates assimilating paleoclimate history: new implications for the thermochemical structure of Ireland, *J. geophys. Res.: Solid Earth,* **123**(12), 10 951–910 967.

Mather, B. & Fullea, J. 2019. Constraining the geotherm beneath the British Isles from Bayesian inversion of Curie depth: integrated modelling of magnetic, geothermal, and seismic data, *Solid Earth,* **10**(3), 839–850.

Meere, P.A. & Banks, D.A. 1997. Upper crustal fluid migration: an example from the Variscides of SW Ireland, *J. Geol. Soc.,* **154,** 975–985. https://www.lyellcollection.org

Meere, P.A., Mulchrone, K.F. & Timmerman, M. 2013. Shear folding in low-grade metasedimentary rocks: reverse shear along cleavage at a high angle to the maximum compressive stress, *Geology,* **41**(8), 879–882.

Meier, T., Dietrich, K., Stöckhert, B. & Harjes, H.P. 2004. One-dimensional models of shear wave velocity for the eastern Mediterranean obtained from the inversion of Rayleigh wave phase velocities and tectonic implications, *Geophys. J. Int.,* **156**(1), 45–58.

Mertoglu, O., Simsek, S., Basarir, N. & Paksoy, H. 2019. *Geothermal Energy Use, Country Update for Turkey*. European Geothermal Congress 2019 Den Haag.

Mitchell, W.I.(Ed.). 2004. *The Geology of Northern Ireland. Our Natural Foundation*(2nd ed.). Geological Survey of Northern Ireland.

Möllhoff, M. & Bean, C.J. 2016. Seismic noise characterization in proximity to strong microseism sources in the Northeast Atlantic, *Bull. seism. Soc. Am.,* **106**(2), 464–477.

Naylor, D. 1992. The post-Variscan history of Ireland, in *Basins on the Atlantic Seaboard: Petroleum Geology, Sedimentology and Basin Evolution,* 62ndedn, Vol., **62,** pp. 255–275, ed. Parnell, J. Geological Society. https://www.lyellcollection.org

Nolet, G., 2008. *A Breviary of Seismic Tomography*. Cambridge Univ. Press, pp. 324.

O'Donnell, J.P., Daly, E., Tiberi, C., Bastow, I.D., O'Reilly, B.M., Readman, P.W. & Hauser, F. 2011. Lithosphere-asthenosphere interaction beneath Ireland from joint inversion of teleseismic *P*-wave delay times and GRACE gravity, *Geophys. J. Int.,* **184**(3), 1379–1396.

O'Reilly, B.M., Hauser, F., Ravaut, C., Shannon, P.M. & Readman, P.W. 2006. Crustal thinning, mantle exhumation and serpentinization in the Porcupine Basin, offshore Ireland: evidence from wide-angle seismic data, *J. Geol. Soc.,* **163**(5), 775–787.

O'Reilly, B.M., Hauser, F. & Readman, P.W. 2010. The fine-scale structure of upper continental lithosphere from seismic waveform methods: insights into Phanerozoic crustal formation processes, *Geophys. J. Int.,* **180**(1), 101–124.

O'Reilly, B.M., Hauser, F. & Readman, P.W. 2012. The fine-scale seismic structure of the upper lithosphere within accreted Caledonian lithosphere: implications for the origins of the "Newer Granites," *J. Geol. Soc.,* **169**(5), 561–573.

O'Reilly, B.M., Kiyan, D., Fullea, J., Lebedev, S., Bean, C.J., Meere, P.A. & Chambers, E.L. 2021. *DIG: A New Project to De-risk Ireland's Geothermal Energy Potential*. EGU General Assembly. EGU–12254.

Parkes, D., Busby, J., Kemp, S.J., Petitclerc, E. & Mounteney, I. 2020. The thermal properties of the Mercia Mudstone Group, *Q. J. Eng. Geol. Hydrogeol.,* **54**(2),.

Pasquali, R., Allen, A., Burgess, J., Jones, G.L. & Williams, T.H. 2015. Geothermal Energy Utilisation-Ireland Country Update, *Proceedings World Geothermal Congress 2015,* Melbourne, Australia, 19-25 April 2015. https://pangea.stanford.edu/ERE/db/WGC/papers/WGC/2015/01043.pdf

Pasquali, R., O'neill, N., Reay, D. & Waugh, T. 2010. The Geothermal Potential of Northern Ireland, In *Proceedings World Geothermal Congress 2010,* Bali, Indonesia, 25-29 April 2010.

Pearson, D.G., Canil, D. & Shirey, S.B., 2003. Mantle samples included in volcanic rocks: xenoliths and diamonds, in *Treatise on Geochemistry,* Vol., **2,** pp. 171–275, ed. Carlson, R.W., Holland, H.D. & Turekian, K.K., Elsevier, ISBN 0-08-043751-6.

Piana Agostinetti, N. & Licciardi, A. 2015. SIM-CRUST Project—Seismic Imaging and Monitoring of the Upper Crust : exploring the Potential Low-Enthalpy Geothermal Resources of Ireland, *Proceedings World Geothermal Congress 2015,* Melbourne, Australia 19-25 April 2015.

Polat, G., Lebedev, S., Readman, P.W., O'Reilly, B.M. & Hauser, F. 2012. Anisotropic rayleigh-wave tomography of Ireland's crust: implications for crustal accretion and evolution within the caledonian orogen, *Geophys. Res. Lett.,* **39**(4), 1–5.

Popov, Y., Beardsmore, G., Clauser, C. & Roy, S. 2016. ISRM suggested methods for determining thermal properties of rocks from laboratory tests at atmospheric pressure.,*Rock Mech. Rock Eng.,* **49**(10), 4179–4207.

Poulsen, S.E., Balling, N., Bording, T.S., Mathiesen, A. & Nielsen, S.B. 2017. Inverse geothermal modelling applied to Danish sedimentary basins, *Geophys. J. Int.,* **212**(1), 389–389.

Poulsen, S.E., Balling, N. & Nielsen, S.B. 2015. A parametric study of the thermal recharge of low enthalpy geothermal reservoirs, *Geothermics,* **53,** 464–478.

Quinn, M.F. 2006. *Lough Neagh: the site of a Cenozoic pull-apart basin*, *Scottish J. Geol.,* **42**(2), 101–112.

Raine, R. & Reay, D. 2019. *A Review of Geothermal Reservoir Properties of Triassic, Permian and Carboniferous sandstones in Northern Ireland (Geological Survey of Northern Ireland Internal Report 19/EM/01),* British Geological Survey. Available at: www.bgs.ac.uk/gsni

Reay, D.M. 2004. Geophysics and concealed geology, in *The Geology of Northern Ireland, Our Natural Foundation,* pp. 227–248, ed. Mitchell, W. I., The Geological Survey of Northern Ireland.

Reinecker, J., Gutmanis, J., Foxford, A., Cotton, L., Dalby, C. & Law, R. 2021. Geothermal exploration and reservoir modelling of the united downs deep geothermal project, Cornwall (UK), *Geothermics,* **97,** 102226.

Scheck-Wenderoth, M., Cacace, M., Maystrenko, Y.P., Cherubini, Y., Noack, V., Kaiser, B.O., Sippel, J. & Björn, L. 2014. Models of heat transport in the Central European Basin System: effective mechanisms at different scales, *Mar. Pet. Geol.,* **55,** 315–331.

Scheck-Wenderoth, M. & Maystrenko, Y.P. 2013. Deep control on shallow heat in sedimentary basins, *Energy Proc.,* **40,** 266–275.

Serpen, U. & DiPippo, R. 2022. Turkey—A geothermal success story: a retrospective and prospective assessment, *Geothermics,* **101,** 102370.

ShallowTHERM. 2021. *ShallowTHERM,* ShallowTHERM Webpage. http://irishgroundtherm.com/results-2/

Shannon, P.M. 2018. Old challenges, new developments and new plays in Irish offshore exploration, *Petrol. Geol. Conf. Proc.,* **8**(1), 171–185.

Somerton, W.H. 1992. Chapter V. Thermal conductivity of rock/fluid systems, in *Thermal Properties and Temperature-related Behavior of Rock/fluid Systems,* Vol., **37,** pp. 39–81, ed. Somerton, W. H., Elsevier.

Stixrude, L. & Lithgow-Bertelloni, C., 2011. Thermodynamics of mantle minerals-II. Phase equilibria, *Geophys. J. Int.,* **184,** 1180–1213.

Torne, M. *et al.* 2023. Advances in the modeling of the Iberian thermal lithosphere and perspectives on deep geothermal studies, *Geothermal Energy,* **11**(1), 3.

van den Berg, R., Daly, J.S. & Salisbury, M.H. 2005. Seismic velocities of granulite-facies xenoliths from Central Ireland: implications for lower crustal composition and anisotropy, *Tectonophysics,* **407**(1–2), 81–99.

Vilà, M., Fernández, M. & Jiménez-Munt, I. 2010. Radiogenic heat production variability of some common lithological groups and its significance to lithospheric thermal modeling, *Tectonophysics,* **490**(3–4), 152–164.

Vozar, J., Jones, A.G., Campanya, J., Yeomans, C., Muller, M.R. & Pasquali, R. 2020. A geothermal aquifer in the dilation zones on the southern margin of the Dublin Basin, *Geophys. J. Int.,* **220**(3), 1717–1734.

Wawerzinek, B., Ritter, J.R.R., Jordan, M. & Landès, M. 2008. An uppermantle upwelling underneath Ireland revealed from non-linear tomography, *Geophys. J. Int.,* **175**(1), 253–268.

Wheildon, J., Gebski, J.S. & Thomas-Betts, A. 1985. *Further Investigations of the UK Heat Flow Field (1981-1984),* Report, British Geological Survey, contract EG-A1-041-80-UK (H), WJ/GE/85/1

Willmot Noller, N.M. & Daly, J.S. 2015. The Contribution of Radiogenic Heat Production Studies to Hot Dry Rock Geothermal Resource Exploration in Ireland, *World Geothermal Congress 2015, April,* 19–25.

Woodcock, N. & Strachan, R.A. 2009. *Geological History of Britain and Ireland*. John Wiley and Sons.

Yeomans, C.M. 2011. *Geothermal implications of the Mourne Mountains: constraints from magnetotelluric modelling*[Masters Thesis]. University of Birmingham.

Younger, P.L., Gluyas, J.G. & Edryd Stephens, W. 2012. Development of deep geothermal energy resources in the UK, *Energy,* **165**(EN1), 19–32.